Implications of in situ calcification for photosynthesis in a 3.3 Ga-old microbial biofilm from the Barberton greenstone belt, South Africa

Francès Westall, Barbara Cavalazzi, Laurence Lemelle, Yves Marrochi, Jean-Noël Rouzaud, Alexandre Simionovici, Murielle Salomé, Smail Mostefaoui, Caroline Andreazza, Frédéric Foucher, et al.

Implications of *in situ* calcification for photosynthesis in a ~3.3 Ga-old microbial biofilm from the Barberton greenstone belt, South Africa

Frances Westall[1*], Barbara Cavalazzi[1,14], Laurence Lemelle[2], Yves Marrocchi[3], Jean-Noël Rouzaud[4], Alexandre Simionovici[5], Murielle Salomé[6], Smail Mostefaoui[3], Caroline Andreazza[7], Frédéric Foucher[1], Jan Toporski[8], Andrea Jauss[8], Volker Thiel[9], Gordon Southam[10], Lachlan MacLean[10], Susan Wirick[11], Axel Hofmann[12], Anders Meibom[3], François Robert[3], Christian Défarge[13]

[1]Centre de Biophysique Moléculaire-CNRS-OSUC, Rue Charles Sadron, 45071 Orléans cedex 2, France. Frances.westall@cnrs-orleans.fr

[2]Université de Lyon, CNRS, UMR5276-Laboratoire de Géologie de Lyon, USR3010-Laboratoire Joliot-Curie, Ecole Normale Supérieure de Lyon, 46 allée d'Italie – 69007 Lyon, France. laurence.lemelle@ens-lyon.fr

[3]Laboratoire d'Etude de la Matière Extraterrestre, Muséum National d'Histoire Naturelle, 61, rue Buffon, 75005 Paris, France. marrocchi@mnhn.fr

[4]Laboratoire de Géologie de l'Ecole Normale Supérieure, CNRS UMR8538, 24 Rue Lhomond, 75231 Paris CEDEX 5, France. rouzaud@mailhost.geologie.ens.fr

[5]Laboratoire de Géodynamique des Chaînes Alpines, Observatoire des Sciences de l'Univers de Grenoble, Maison des Géosciences, BP 53, 38041 Grenoble Cedex 9, France. alexandre.simionovici@ujf-grenoble.fr

[6]ID21 Beamline, European Synchrotron Radiation Facility (ESRF), 6 rue J. Horowitz, F-38043 Grenoble Cedex, France. salome@esrf.fr

[7]Centre de Recherche sur la Matière Divisée, 1b rue de la Férollerie, 45071 Orléans Cedex 2 France. caroline.andreazza@univ-orleans.fr

[8]WITec Wissenschaftliche Instrumente und Technologie GmbH, Hörvelsinger Weg 6, D-89081 Ulm, Germany. jan.toporski@witec.de

[9]Geobiology Group, Geoscience Center, Georg-August University of Göttingen, Goldschmidtstr. 3 , 37077 Göttingen, Germany. vthiel@gwdg.de

[10]Department of Earth Sciences, University of Western Ontario, 1151 Richmond St, London, Ontario, N6A 5B7 Canada. gsoutham@uwo.ca

[11]Physics and Astronomy Dept. SUNY at StonyBrook, StonyBrook, NY 11794, USA. swirick@bnl.gov

[12]Department of Geology, University of Johannesburg, Auckland Park 2006, Johannesburg, South Africa. ahofmann@uj.ac.za

[13]Université d'Orléans/ Université François Rabelais - Tours – CNRS/INSU, Institut des Sciences de la Terre d'Orléans, UMR 6113, Polytech'Orléans, 45067 Orléans cedex 2, France. christian.defarge@univ-orleans.fr

[14]Department of geology, University of Johannesburg, Kingsway Campus, PO Box 524 Auckland Park 2006 South Africa. cavalazzib@uj.ac.za

Corresponding author

Frances Westall

Centre de Biophysique Moléculaire, CNRS, Rue Charles Sadron, 45071 Orléans cedex 2, France

Frances.westall@cnrs-orleans.fr

Tel +33 238 257912 ; or +33 632 458 523

Fax: +33 238 631517

Highlights

- *In situ* calcification (aragonite) of a 3.3 Ga microbial biofilm
- Calcification probably due to the activities of a photosynthetic consortium of microorganisms within the biofilm including heterotrophic sulphur reducing bacteria
- Preservation of the metastable carbonate phase by the organic matrix and secondary silicification
- Oldest known occurrence of aragonite.

ABSTRACT

Timing the appearance of photosynthetic microorganisms is crucial to understanding the evolution of life on Earth. The ability of the biosphere to use sunlight as a source of energy (photoautotrophy) would have been essential for increasing biomass and for increasing the biogeochemical capacity of all prokaryotes across the range of redox reactions that support life. Typical proxies for photosynthesis in the rock record include features, such as a mat-like, laminated morphology (stratiform, domical, conical) often associated with bulk geochemical signatures, such as calcification, and a fractionated carbon isotope signature. However, to date, *in situ*, calcification related to photosynthesis has not been demonstrated in the oldest known microbial mats. We here use *in situ* nanometer-scale techniques to investigate the structural and compositional architecture in a 3.3 billion-year (Ga) old microbial biofilm from the Barberton greenstone belt, thus documenting *in situ* calcification that was most likely related to anoxygenic photosynthesis. The Josefsdal Chert Microbial Biofilm (JCMB) formed in a littoral (photic) environment. It is characterised by a distinct vertical structural and compositional organisation. The lower part is calcified *in situ* by aragonite, progressing upwards into uncalcified kerogen characterised by up to 1% sulphur, followed by an upper layer that contains intact filaments at the surface. Crystallites of pseudomorphed pyrite are also associated with the biofilm suggesting calcification related to the activity of heterotrophic sulphur reducing bacteria. In this anoxygenic, nutrient-limited environment, the carbon required by the sulphur reducing bacteria could only have been produced by photoautotrophy. We conclude that the Josfsdal Chert Microbial Biofilm was formed by a consortium of anoxygenic microorganisms, including photosynthesisers and sulphur reducing bacteria.

Keywords

Barberton, microbial mat, photosynthesis, calcification, aragonite

1. INTRODUCTION

The earliest traces of photosynthesis occur in well-preserved sedimentary rocks of Early-Mid Archaean age (4.0-3.3 Ga) in the Barberton (South Africa) and Pilbara (Australia) greenstone belts (see review in Westall, 2010). In the commonly accepted understanding of the evolution of life, anoxygenic photosynthetic microorganisms appeared first in the Early-Mid Archaean (Tice and Lowe, 2004; Westall et al., 2006) while the more sophisticated and more efficient oxygenic photosynthesisers appeared in the Late Archaean (Buick, 1992; Altermann and Schopf, 1995; Brocks et al., 1999; Summons et al., 1999).The most common expression of photosynthesis in the rock record is fossilised photosynthetic microbial mats. These are finely laminated structures that are formed by photosynthetic microorganisms in generally oligotrophic environments where the primary producing microorganisms have access to sunlight that they can use as an energy source. These mats are highly complex consortia of different kinds of microorganisms living off the organic biomass produced initially by the photosynthetic microorganisms (Dupraz et al., 2009). The preservation of photosynthetic microbial mats is serendipitous because they often form in ephemeral, littoral environments that are active and subject to physical destruction (Noffke, 2009). Moreover, early diagenetic processes may also lead to complete degradation of the mats or blurring of their signatures. A concatenation of events is therefore required to preserve them, such as burial by fine detritus to produce recognisable, microbially-influenced sedimentary structures (MISS, Noffke, 2009), or impregnation of the layered photosynthetic structure by minerals, such as carbonate or silica (Walter, 1976; Cady and Farmer, 1996; Konhauser et al., 2001; Jones et al., 2001). The latter process will concomitantly dilute any organic or geochemical proxy signature.

Given the vagaries of the taphonomic process, identification of the remains of photosynthetic microbial mats in ancient rocks needs to be based on a range of

complementary data that support its formation within the photic zone, as well as identifying proxies that indicate that the mat was formed by photosynthetic microorganisms. Proxy features that are commonly used to identify fossil photosynthetic microbial mats include (1) a mat-like, laminated morphology (planar or three dimensional, as in domical or columnar stromatolites), (2) the presence of fossil microorganisms of known photosynthetic affinity (e.g., the later-evolved oxygenic photosynthesising cyanobacteria, many species of which have readily identifiable morphologies), (3) a carbon isotopic signature consistent with photosynthesis, (4) evidence of *in situ* calcification as a by-product of photosynthetic activity (Supplementary figure 1). It should also be demonstrated that these combined characteristics do not occur in microbial mats formed by non-photosynthesising microorganisms. Bailey et al (2009) note that almost all of the physical and chemical characteristics used for identifying fossil photosynthetic mats can also be produced by non-photosynthetic mats, such as those formed by sulphur/sulphate or methane oxidisers in cold seep, hydrothermal or other types of environments. Table 1 compares the characteristics of modern photosynthetic and non photosynthetic microbial mats, underlining the similarities between them in terms of environment of formation, structure, composition and metabolic signatures.

Both types of mats can be formed in the photic zone but non-photosynthetic mats can also form in caves or deep water. Both can form on sediment surfaces but non-photosynthetic mats also form within the sediment. Both mat types can be laminated (chemical mineral precipitates, such as calcareous travertines can also be laminated, Pentecost, 2005). Whereas non-photosynthetic microbial mats have also been described as being sediment stabilising and having crenulated, contorted and wrinkled surface (Bailey et al., 2009). However, interlayering with chemically-precipitated evaporite deposits in littoral/sabkha environments seems to be restricted to photosynthetic mats. Certain biomarkers distinguish the microbial composition of photosynthetic and non-photosynthetic microbial mats. For example,

Summons et al., (1999) describe 2-methylhopanes from 2.7 Ga-old oil shales from the Pilbara of Australia as being the degradation products of phototrophic bacterial lipids. Lipid biomarkers of sulphate reducing bacteria include mono-O-alkyl glycerol ethers (Arning et al., 2008). However, biomarkers have a limited life time (albeit very long) and even at 2.7 Ga the syngenicity of the 2-methylhopanes is questioned (Rasmussen et al., 2008). Elemental sulphur deposits are associated with mats formed by sulphur-oxidising bacteria (Nelson and Castenholz, 1981) but not with photosynthetic microbial mats. Phosphorite deposits are also characteristic of non-photosynthetic microbial mats, such as those formed by the sulphur-oxidisers *Beggiatoa* (Reimers et al., 1990) and *Thiomargarita* (Schultz et al., 1999). Calcification, on the other hand, occurs in non-photosynthetic microbialites, such as carbonate mud mounds formed around cold seeps (Barbieri and Cavalazzi, 2005), as well as in photosynthetic microbial mats (Dupraz et al., 2009).

Although many species of cyanobacteria are readily recognisable in the fossil record when well preserved (e.g., Hofmann, 1976; Knoll, 1985), not all photosynthetic microorganisms possess distinct morphological attributes and not all microorganisms can be/are fossilised (Westall, 1997; Orange et al., 2009). Carbon isotope signatures are not sufficiently distinctive of photosynthesis since photosynthetic microorganisms are characterised by a wide range of $\delta^{13}C$ values (e.g., -3 to -28‰ for oxygenic photosynthesisers and -9 to -36‰ for anoxygenic photosynthesisers) that overlap with those of other non-photosynthetic microorganisms (Schidlowski, 1988, 2001), as well as those of carbon formed by non-biogenic processes (van Zuilen et al., 2002). However, bulk carbon isotope signatures from photosynthetic microbial mats will be heavier than those for mats produced by sulphur/sulphate oxidisers or methane oxidisers. Moreover, carbon isotopic measurements are generally made on bulk rock samples that contain traces of the hypothetical photosynthetic

microbial mats, as well as traces of any other microorganisms in that particular habitat. The resulting isotopic signature will, thus, be mixed.

Purported photosynthetically metabolising microorganisms and their macrostructures (microbial mats, stromatolites) have been identified in the oldest, well-preserved sedimentary rocks known. Dunlop et al. (1978), Schopf and Walter (1983), and Lowe (1980, 1983) first described stromatolites and/or the possible remains of cyanobacteria in well-preserved sediments (cherts) dating from the Early Archaean (3.5-3.3 Ga) in the Pilbara region of NW Australia. Similar interpretations were made in Early Archaean cherts from the Barberton greenstone belt in South Africa (Byerly et al., 1986). Further studies have been undertaken since the 1990s in both Early Archaean terrains (e.g. Walsh, 1992; Schopf, 1993; Hofmann et al., 1999; Tice and Lowe, 2004, 2006; Allwood et al., 2006, 2009; Tice, 2009; Westall et al., 2001, 2006; see reviews by Westall, 2004, 2010) using structure (laminated and/or domical), and fractionated carbon isotopic signatures as proxies for photosynthesis. The remains of the photosynthetic primary producing organisms are rarely preserved (cf. Altermann and Schopf, 1995), Indeed, the carbon isotope signatures of highly metamorphosed sediments from the Isua Greenstone belt in Greenland (3.8 Ga) were also interpreted as indications of photosynthesis (Schidlowski, 1988, 2001; Mojzsis et al., 1996; Rosing, 1999). Critiques of some of the studies have concentrated on the biogenicity of the laminated structures (Lowe, 1994; Brasier et al., 2002) and the hypothetical photosynthetic isotopic signatures (e.g. van Zuilen et al., 2002). More recent investigations have addressed the importance of environmental habitat and the effects of local variations on the distribution of the ancient photosynthetic structures. For instance, Allwood et al. (2006,2009) demonstrated by detailed field mapping and macro to microscopic analyses that several varieties of domical structures in a 3.5 Ga-old formation in the Pilbara in Australia formed in a variety of localised habitats on a shallow water carbonate platform. They argued that their environment of formation and their physical and chemical characteristics of the domical structures could only have been produced by photosynthetic microorganisms. Similarly, Tice and Lowe (2004, 2006) and Tice (2009) made a detailed microscopic and isotopic study of laminated structures in the 3.4 Ga-

old Kromberg Formation in the Barberton Greenstone Belt, interpreted in terms of a diversity of mats related to specific local environments in a littoral environment.

Among all proxies, *in situ* calcification, which is a common signature of modern, lithifying photosynthetic microbial mats (Supplementary figure 1; Défarge et al., 1994, 1996; Dupraz et al., 2009), is one feature that remains un-documented in these ancient putative microbial ecosystems. The objective of our study is therefore to present evidence of *in situ* calcification in a microbial biofilm and microbial mats present in a 3.3 Ga-old sediment from the Josefsdal Chert Formation in the Barberton Greenstone Belt, South Africa, and to examine the relationship between calcification and the possible photosynthetic origin of the biofilm and mats. With this in view, we present an *in situ* structural and compositional analysis of the biofilm and mats on a micrometric microbial scale. Our approach mimics, as closely as possible, that used in the study of modern photosynthetic microbial mats in which a range of observational, geochemical, metabolic, and genetic methods are used at the microbial mat scale.

2. GEOLOGICAL BACKGROUND, MATERIALS AND ANALYTICAL METHODS

2.1. Geological Context

The Early to Mid Archaean Barberton greenstone belt of South Africa contains some of the world's oldest and best-preserved supracrustal sequences that provide a wealth of information on Earth's history and early life (e.g., Byerly et al., 1986; Walsh, 1992; Banerjee et al., 2006; Westall et al., 2006; Tice, 2009). The belt consists of a NE-SW striking succession of supracrustal rocks, termed the Barberton Supergroup (or Swaziland Supergroup in the older literature), which ranges in age from ~3550 to 3220 Ma. The belt has a strike length of ~130 km, width of 10-35 km, and an approximate depth of 4-5 km, and is surrounded by granitoid domes and intrusive sheets, ranging in age from ~3.5 to 3.1 Ma. The

volcano-sedimentary sequence of the Barberton greenstone belt has been subdivided into three stratigraphic units, the Onverwacht, Fig Tree and Moodies Groups (SACS, 1980). The study locality consists of two chert horizons cropping out in the topmost of the Kromberg Formation of the Onverwacht Group in the upper part of the Josefsdal Valley (S25°57'54", E31°04'41", Figure 1). Based on its occurrence at the top of Onverwacht Group between the top of the Kromberg Formation and the Mendon Formation (Figure. 1b), the age of the Josefsdal Chert is estimated at ~3.3 Ga. The Josfsdal Chert underwent regional greenschist metamorphism dated at 3.32 Ga (Dziggel et al., 2002).

The study outcrop consists of banded black and white/greenish white silicified volcaniclastic sediments deposited on top of pillow basalt (Supplementary Figure 2). Sedimentary structures in the chert indicate deposition in water depths ranging from sub wave base to shallow water. The black horizons contain organic matter and pseudomorphed pyrite crystals (now iron oxide), the organic matter consisting of organic detritus as well as occasional laminated microbial mats (Supplementary Figure 3). The samples used in this study come from a horizon stratigraphically located at the base of the silicified sediments.

We have based our study on microbial mat-like structures observed in thin section and in cut rock surfaces of Josefsdal Chert, and, in particular, on an exceptionally well-preserved microbial biofilm exposed in three dimensions directly on top of a bedding plane surface. A preliminary description of the exposed microbial biofilm, henceforth termed the *Josefsdal Chert Microbial Biofilm* (JCMB) in this work, was made by Westall et al. (2001, 2006).

The JCMB occurs on a fresh fracture surface that partially follows a bedding plane between the top of an underlying black (carbon-rich) layer and an overlying greenish white layer. The rock surface on which the biofilm is exposed is uneven and, in a small area, other biofilm fragments alternate with sediment layers deposited above the JCMB (Supplementary figure 4). It consists of portions of a thin carbonaceous film, <10 μm thick, that collectively

cover an area of about 6 mm^2 (Figure 2a; Supplementary Figure 2b). The biofilm is only one of a packet of mat-like structures whose combined thickness is <1 mm (the upper portions were almost entirely removed by fracturing). It is similar to the mat shown in a thin section of the Josefsdal Chert in Supplementary Figure 3. The surface of the film consists of fine filaments, 0.25-0.3 µm in diameter, that are thickly coated with a smooth material interpreted as EPS (Figures 6, 8 in Westall et al., 2006). Parallel orientation of the filaments and overturning of portions of the mat in the same direction (Figures 5 and 6a in Westall et al., 2006) suggest formation under flowing water, possibly close to a hydrothermal spring since the biofilm was silicified *in vivo* by hydrothermal fluids. A subaerial beach setting is suggested by the presence of intercalated layers of pseudomorphed (silicified) evaporite crystals in the upper layers of the film and by cracks in its surface that indicate periodic exposure to the atmosphere (Figure 6d in Westall et al., 2006). Detrital particles including volcanic shards and quartz grains from 10's of µm up to ~300 µm in size are trapped in the mat (Figure 7b in Westall et al., 2006).

Carbon isotope signatures for the bulk sediment were -22.7 ‰ (Westall et al., 2001) and a value of -26.8 ‰ was obtained for a bulk sample of separated carbon-rich black layers (Westall et al., 2006). The turgid filaments in the surface of the biofilm, rather than degraded remnants, (Figures 6f, 8b in Westall et al., 2006) suggest rapid silicification probably by silica-rich hydrothermal fluids as the biofilm was living (cf. Hofmann and Bohlar, 2007). This is supported by the fact that the anions of the evaporite crystals have been replaced by fluorine, most likely present in the same hydrothermal fluids that induced silicification of the mat.

2.2. Analytical techniques

FIB preparations

Most of the analyses made in this study were conducted on a series of focussed ion beam (FIB) sections vertically cut using a Ga beam into the 5-10 µm thick mat (Figure 2b) (Lekstrom et al., 2008). (*N.B.* the mat had previously been coated with Au for SEM observation, Westall et al., 2006). The FIB sections were prepared at the Centre Pluridisciplinaire de Microscopie Electronique et de Microanalyse at the University Aix-Marseille using a Philips FIB 200, and at the Institute d'Électronique, Microélectronique et de Nanotechnologie (IEMN), Lille, using an FEI Strata DB 235. On some sections, a protective 1-2 µm thick platinum strip was deposited on the sample before milling in order to protect the FIB slice. The primary ion currents used for *in situ* milling and polishing of the FIB sections were in the range of 0.17 to 7 nA and beam energies ranged from 2 to 30 keV. Sections 90 nm thick were mounted on Cu-TEM grids coated with holey carbon film were prepared for transmission electron microscope (TEM) analyses, whereas thicker FIB sections of 3µm were prepared for scanning electron microscope (SEM), scanning transmission electron microscopy (STEM), NanoSIMS (a high spatial resolution secondary ion mass spectrometry) and synchrotron radiation analysis.

SEM and TEM

Three TEM instruments used were a Philips CM20 TEM fitted with EDX detector available at Centre de Microscopie Electronique, Université d'Orléans, France; a TEM JEOL 2011 microscope at the University of Paris VI, France; and a FEI TECNAI G2 at the Centre Pluridisciplinaire de Microscopie électronique et de Microanalyse (CP2M), Marseille, France. In all cases, the beam energy used was 200 kV and the microscopes were equipped with a energy-dispersive X-ray spectroscope (EDX) capable of measuring light elements (except for the JEOL 2011 TEM). The SEM instruments used included an Hitachi S4500 FEG-SEM, equipped with a Polaron LT7400 cryopreparation system that can function as a cryoSEM, at

the Centre de Microscopie Electronique, Orléans and a Philips XL30 SFEG STEM at the Centre Pluridisciplinaire de Microscopie Electronique et de Microanalyse at the University Aix-Marseille. SEM imaging and elemental mapping were made between 5-10 kV.

Synchrotron analysis: The beamline ID21 SXM set-up for fluorescence imaging and μ-XANES of S at the K-edge

FIB sections prepared for synchrotron irradiation were mounted on C-coated TEM Cu-grids. With its 2-7 keV energy range, the ID21 scanning X-ray microscope (SXM) of the European Synchrotron Radiation Facility (ESRF) in Grenoble (Susini et al., 2002) is a unique tool for microspectroscopy at the sulfur K-edge, attaining high spatial (0.3 μm) and spectral (0.25 eV) resolution. The SXM was operated at energies around 2472 eV, close to the sulfur K-edge. Micro fluorescence maps were also performed at the Fe K-edge around 7112 eV with a comparable set up. The FIB cuts mounted on TEM grids were held between 4 μm thick Ultralene® foils. The sample is positioned at an angle of 60º (90º between beam and fluorescence detector axis) with respect to the incoming beam. Further details of the instrument setup are provided in the Supplementary Methods.

STXM and Near-Edge X-ray Absorption Fine Structure (NEXAFS) spectroscopy at the C K-edge

Scanning transmission X-ray microscopy (STXM) and Near-Edge X-ray Absorption Fine Structure (NEXAFS) spectroscopy at the C K-edge analyses were made on the X1A beamline at the National Synchrotron Light Source (NSLS, Brookhaven). Data for the Josefsdal Chert were collected using a STACK data collection technique where an image is taken, the monochromator energy is changed by a small increment; another image is collected and so on until a series of images over the energy range of interest is collected. The images

are aligned in X and Y using a cross correlation algorithm. Spectra can be obtained from individual pixels in the image. Carbon maps are acquired by taking the difference of the sum of images acquired below 283 eV and the sum of images acquired between 290-293 eV. The STACK energy spacing for this data set was 280-283.6 eV, with 0.3 eV step size, 283.6-292.0 eV with 0.1 eV step size, 292-305 eV with 0.3 eV step size (Jacobsen, et al, 2000). The image size was 320 pixels in both X and Y with a pixel size of 30nm. Further details of the instrument setup are provided in the Supplementary Methods.

NanoSIMS

Chemical maps of a 10 x 3 x 15 μm FIB section were produced with the Cameca NanoSIMS 50 at the Muséum National d'Histoire Naturelle in Paris, France (*N.B.* the same FIB section was analysed by μ-XANES at the ESRF, Grenoble). The instrument is characterized by high spatial resolution (down to 50 nm), high sensitivity, and the simultaneous detection of up to five isotopes. In this study, negative secondary ions of ^{12}C, ^{16}O, $^{12}C^{14}N$, ^{28}Si and ^{32}S were mapped simultaneously (multicollection-mode) using electron-multiplier detectors. Using primary current conditions (about 0.5 pA on the sample surface), the primary ion beam of Cs^+ was focused onto the sample in spots <100 nm in size. Analyses were performed at a mass-resolving power > 5000, sufficient to resolve significant isobaric interferences. A normal incidence electron gun was tuned during analysis in order to compensate for positive primary beam charge deposition on the sample surface. Two ion images consisting of 256 x 256 pixels were acquired by scanning areas of 17 x 17 μm and with counting times of 1 s/pixel. Within the imaged regions, two oxygen-rich features were observed and subsequently imaged in frames of 8 x 8 μm (256 x 256 pixels) and with a spatial resolution of about 50 nm. Note that, because nitrogen can only be detected as CN^- in NanoSIMS, it can only be measured in the presence of carbon. Also, the sample was attached

to a metallic mount using carbon tape, which greatly reduces the risk of surface contamination compared to the use of epoxy.

ToF-SIMS

The Time-of-Flight Secondary Ion Mass Spectroscopy (ToF-SIMS) analyses were made on a cleaned cut rock surface using an ION-TOF IV GmbH instrument (Münster, Germany) equipped with a Bismuth liquid metal primary cluster ion source (see details below) at the Technical Research Institute of Sweden (Borås). Spectra from the sections were recorded using 25 keV Bi_3^+ primary ions, with the instrument optimized for maximum mass resolution (bunched mode, $m/\Delta m$ ~3000–6000). The cleaning protocol for the samples is as follows. The rock surface was sawn with saw blades that had been thoroughly cleaned and rinsed with acetone. MilliQ water was used during sawing. The outer portions of the rock sample were sawn off and discarded to eliminate contamination. A slice of rock from the inside of the hand specimen was then sawn, wrapped in acetone-cleaned aluminium foil and stored in a cooled Ar-filled, Schott glass container until analysed. The sample was removed from the container in a laminar flow hood, placed on the ToF-SIMS sample holder, and then placed directly in the instrument for analysis.

Raman spectrometry

Raman spot analyses and mineralogical maps of a polished thin section of the Josefsdal Chert were carried out using a WITec Alpha500 RA system. The light source used was a frequency-doubled Nd:YAG green laser (wavelength λ=532 nm). Low energy power of ~6 mW was used in order to prevent deterioration of the samples.

3. RESULTS

Microbial mats in thin section

Microbial mat-like structures were observed in a number of thin sections from the Josefsdal Chert outcrop. They occur as packets of fine anastomosing laminae tens of micrometers in thickness (Supplementary Figure 3). The laminae are conformable with the underlying surface but have a wispy, undulating structure. They trap detrital particles such as quartz and volcanic grains. The laminae form packets that can be up to several hundred micrometers in thickness suggesting some periodicity to growth. Raman spectral mapping documented their kerogenous composition (Supplementary Figure 5) (D:G peak ratio of about 2.5). Analysis and mapping using an ion probe demonstrated that they are enriched in Ca, a result which triggered further investigation of the Ca-containing phase. Small crystals of pseudomorphed pyrite (1-2 μm) are frequently associated with the black layers (Supplementary Figure 5b). Although now oxidised, EDX and μ-XANES analyses document remnant sulphur in the crystals (data not shown).

ToF-SIMS analysis on the carbonaceous layers (Supplementary Figure 6) in the hand specimen identified molecules including $C_7H_7^+$ (tropylium) at 91.05m/z; $C_9H_7^+$ at 115.05 m/z; $C_{10}H_8^+$ (naphthalene) at 128.06 m/z; and the largest molecule, $C_{14}H_{10}^+$ (anthracene/phenanthrene) at 178.06 m/z.

The Josefsdal Chert fossil Microbial Biofilm

There are two distinct types of carbonate phases associated with the JCMB. Silicified pseudomorphs after calcite are part of the evaporite mineral suite interbedded and coating the topmost layers of the filamentous biofilm (Figure 3; Figures 6c,d in Westall et al., 2006). The silicified pseudomorphs of calcite in the top part of the biofilm are blocky crystals, 5-10 μm in size, possessing no other associated elements (Figure 4). There is also a nanocrystalline

phase containing traces of Mg, Fe, Cr and sulphate precipitated in association with the kerogen in the body of the biofilm (Figures 4-6).

Numerous FIB-sections cut vertically through the JCMB show that the 10 µm thick structure is divided into a lower part having a nanometer scale granular texture and an upper part consisting of alveolar-textured kerogen (Figures 3, 5a). The thickness of the kerogen layers varies laterally within the biofilm from < 1 µm to a few micrometers, whereas the granular layer is typically thicker and can be up to about 5 µm (e.g., Figure 3b). High resolution images of the FIB sections show that the 5-10 nm nanocrystals in the lower part of the biofilm have nucleated within an alveolar-textured organic matrix that is structurally similar to that in the overlying kerogen layer (Figures 5, 6; Supplementary Figure 7). Micro-XRF, EDX and µ-XANES mapping of the FIB sections document the association of Ca, Mg, Fe, Cr and sulphate with the nanocrystalline phase, with Ca the predominant element (Figure 4). HRTEM images of the carbonate crystallites (Figure 6) show interplanar distances of 0.335 nm, corresponding to the d_{111} interplane of the carbonate phase aragonite. Fast Fourier Transform imaging of the nanocrystals (inset, Figure 6b) shows a cloudy-spotty ring (corresponding to d = 0.335 nm), typical of the diffraction pattern generated by multiple crystallites with variable rotational orientation.

Elemental mapping by EDX and NanoSIMS show that carbon is ubiquitous throughout the biofilm, and that it occurs especially in the pure kerogen zone in the upper layer of the biofilm, as well as in certain nanocrystal-free pockets within the granular lower part (Figure 7). Traces of N and S are associated with the kerogen. Using µ-XANES we were able to qualitatively estimate up to 1% S in the upper, non-granular portion of the biofilm where both µ-XANES and NEXAFS documented the presence of the S-containing heterocyclic molecule thiophene (Figure 8; Supplementary Figure 8). Note that although the kerogen has an amorphous appearance, HR-TEM shows that, in terms of its nanostructure, it

corresponds to a disordered poly-aromatic carbon containing small stacks of fringes ~1 nm long (Figure 5b), indicating that the kerogen is relatively mature. The molecular moieties identified by ToF-SIMS analyses (Supplementary Figure 8) could correspond to these polyaromatic structures.

4. DISCUSSION

4.1. Timing of the formation of the JCMB

The nanostructure and composition of the organic carbon is consistent with degraded ancient organic carbon that has undergone lower greenschist facies metamorphism, thus indicating that the carbon predates the 3.2 Ga-old metamorphic event that affected the region (Dziggel et al., 2002). While Wacy (2010) suggested that the JCMB might be a later endolithic biofilm supported by a hydrothermal intrusion into the Early Archaean chert, morphological and environmental evidence (Westall et al., 2006) suggest syngenetic formation of the biofilm on a sediment surface in an evaporitic littoral environment. Moreover, the JCMB is part of a packet of biofilms (Supplementary Figure 4) and shares many of the same characteristics as other delicate sediment stabilising microbial mats observed in thin sections of other samples of the Josefsdal Chert (Supplementary Figure 3, see Westall et al., 2006). The syngenicity of its development and calcification is further corroborated by the geochemical data presented here which indicate that the calcification of the JCMB is related to the activities of a photosynthetic consortium that includes sulphur reducing bacteria. The rationale for this interpretation is explained below.

4.2. Calcification of the JCMB

Two, clearly distinct carbonate phases are associated with the JCMB: (1) nanophase aragonite crystals that nucleated onto the alveolar kerogen within the body of the biofilm and

(2) blocky calcite crystals (now pseudomorphed by silica) in the uppermost layer of the JCMB. In terms of crystallography, elemental composition and occurrence, the two phases exhibit different characteristics presumably reflecting different origins. The blocky calcite crystals are large and sub-euhedral relative to the nanophase aragonite. They contain no associated elements apart from Ca and are strictly associated with the suite of pseudomorphed evaporite minerals in the uppermost layers of the JCMB. In contrast, the aragonite crystals are small (5-10 nm), anhedral (spherical to oval in shape), contain traces of Mg, Fe and Cr and sulphate, and occur only in association with the alveolar kerogen within the body of the mat. This phase is always separated from the biofilm surface (and the exterior environment) by a layer of more or less pure kerogen. Calcification of the degraded organic matter in the body of the mat must have occurred as the mat was living because the biofilm was silicified while it was active (the silicified filaments on top of the mat are non-calcified have a turgid morphology, cf. Westall et al., 2006). Nucleation and preservation of 5-10 nm-sized aragonite crystallites within the 'degraded' alveolar kerogen below suggests mediation by the organic matrix in the calcification process, that is, "organomineralisation" *sensu* Défarge et al. (1996) and Défarge (2011). These observations corroborate the syngenicity of the development of the mat and its calcification.

The preservation of aragonite also argues in favour of syngenicity of calcification and JCMB formation. Aragonite is an unstable phase that rapidly converts to calcite and is therefore rare in the geological record (Lepot et al., 2008; Chafetz et al., 2008). Its preservation in the JCMB is probably due to a combination of nucleation within a kerogen matrix (cf. Lepot et al., 2008) and rapid permeation of the biofilm by silica (Figure 9) (cf. Westall et al., 2006, 2010). The formation of aragonite in the EPS of the JCMB rather than another carbonate phase was probably related to its physico-chemical environment of formation. A number of carbonate species may be precipitated during calcification in

microbial mats, including calcite, aragonite, and dolomite although aragonite appears to be the most common form (Bernd and Seyfried, 1999). The presence of primary aragonite in the JCMB is thermodynamically more plausible than calcite because aragonite precipitates instead of calcite at temperatures > 70°C (Kawano et al., 2009). This is consistent with the low temperature hydrothermal setting that gave rise to silicification of the Josefsdal Chert (< 150°C, Hofmann and Harris, 2008). Aragonite is also the favoured Ca-carbonate phase when calcite nucleation and growth are inhibited by the presence of chemical species such as Mg^{2+}, Fe^{2+}, SO_4^{2-} (Berner, 1971; Bischoff and Fyfe, 1968), species which, together with Cr, have been detected in the carbonate of the JCMM. The direct source of these metal ions is probably from early diagenetic alteration of the ultramafic-derived volcaniclastic sediments on top of which the mat formed.

The sequence of events that occurred during the lifetime of the JCMB is summarised in Supplementary Figure 8: (1) biofilm formation on a sediment surface, (2) *in situ* calcification in the lower, degraded part of the film, (3) exposure, desiccation and precipitation of a suite of evaporite minerals on its surface, and (4) final impregnation and coating by hydothermal silica.

Many non-photosynthetic biological mechanisms can lead to calcification, e.g., chemosynthetic systems around cold seeps (Barbieri and Cavalazzi, 2005; Power et al., 2009). Sulphur/sulphate reducing microbial activity and methane oxidation can also lead to carbonate precipitation, as can photosynthesis (the latter only under particular environmental conditions of low dissolved carbon but high Ca; Arp et al., 2001). Carbonate precipitation can also occur through abiological CO_2 degassing and evaporation, for example in travertine. For the JCMB, calcification of the lower layer of the biofilm, below the evaporative surface, suggests the importance of the biosphere in carbonate formation where autotrophy-generated

hydroxyls and subsequent, heterotrophy-generated alkalinity (bicarbonate) contribute to carbonate precipitation.

There are a number of indications that calcification of the JCMB could be related to sulphur reducing bacteria. Sulphur-containing molecules, such as thiophene, occur in the kerogen. Natural bacteriological organic molecules contain sulphur in amounts ranging from 0.4 % (Heldal et al., 2003) to 1% (Fagerbakke et al., 1996). The 1% S in the JCMB kerogen could represent an original composition but may also indicate diagenetic incorporation of sulphur into the organic matrix during anaerobic microbial breakdown of organic matter, such as by sulphur/sulphate-reducing bacteria (sulphurisation; Summons, 1993; Lemelle et al., 2008). Moreover, µm-scale pseudomorphed pyrite crystallites (1-2 µm), a diagnostic by-product of sulphur reducing bacteria activity, are associated with the JCMB and the carbon-rich black layers in the Josefsdal Chert (microbial mats and layers of detrital carbon). As in modern microbial mats (Dupraz et al., 2009), calcification in the JCMB could have occurred in the following manner. The metabolic activity of sulphur reducing bacteria could have caused an increase in dissolved CO_2 within the biofilm, thus increasing the alkalinity. This in turn would have led to desorption of Ca^{2+}ions initially adsorbed to the EPS, which combined with the bicarbonate ions in the water-rich organic matrix. Calcium carbonate would have precipitated from the saturated solutions within the EPS framework and would have fixed to the functional groups on the available organic surfaces (EPS).

4.3 Implications for photosynthesis

The JCMB formed in an anaerobic beach environment. Kasting (1993), modelled 0.2% of present atmospheric levels of O_2 for the Early Archaean period, corroborated by Canfield et al. (2000) who concluded that the early Archaean seawaters were characterised by low sulphate and oxygen concentrations on the basis of the S isotope record. This would

preclude mat formation by aerobic sulphur oxidising microorganisms inhabiting the oxic/anoxic interface (cf. Bailey et al., 2009). The moderately light carbon isotope composition (-26.7‰) indicates that the biofilm was not formed by methane oxidisers. Furthermore, exposure and interlayering with encrusting evaporite minerals in an evaporitic setting is characteristic of photosynthesising mats (although non-photosynthetic mats can co-exist in shallow waters (< 10 cm depth) with photosynthetic mats; Garcia-Pichel et al., 1994). The JCMB is therefore a photosynthetic microbial mat. In the nutrient-limited beach setting in which the Josfsdal sediment formed, the only way to produce the carbon and sulfoxyanions needed by the heterotrophic sulphur reducing bacteria would have been by photoautotrophy. As in modern photosynthetic microbial mats, it is the layered distribution of the carbonate that suggests that this paleo-record of calcification is not the result of a 'pure' culture' but represents a minimum of two complementary metabolic processes, phototrophy and heterotrophy.

Table 1 compares the characteristics of the JCMB with those of modern photosynthesising microbial biofilms. The JCMB formed in the photic zone on an intertidal/supratidal beach surface (cf. Westall et al., 2006) under anaerobic conditions; exhibits direct interaction with it environment in the form of sediment stabilization, formation under flowing water, overturned filaments/mat portions, desiccation (cf. Noffke, 2009; Westall et al., 2006); despite the modest 10 µm thickness, its finely laminated structure with a vertical architecture (degraded lower calcified part, upper non-calcified active layer) is an indication of a steeply changing physico-chemical gradient that can provided micro-environments for a variety of microorganisms having different nutritional requirements and metabolic strategies (Dupraz et al., 2009);; it was formed by EPS-secreting microbial filaments; associated pyrite crystallites and possible sulphurisation most likely indicate sulphur reduction of the primary biomass by heterotrophic bacteria; *in situ* calcification of the

lower part of the mat was probably a by-product of the microbial sulphur-reduction; the moderately light carbon isotope signature of -26.7 ‰ suggests a dominantly phototrophic metabolism.

Thus, despite the ephemeral nature of many of the characteristics of photosynthetic microbial mats, the JCMB still retains fossil signatures that allow it to be interpreted as a photosynthesising microbial mat formed by a consortium of microorganisms with anaerobic photosynthesisers as the primary producers and sulphur reducing bacteria as the heterotrophs.

5. Conclusions

The excellent state of preservation of the 3.3 Ga-old Josefsdal Chert Microbial Biofilm by contemporaneous silicification has permitted three-dimensional, nanometre-scale profiling and imaging that documented, for the first time, *in situ* calcification within a microbial biofilm of this age. Sulphur reducing bacterial activity most likely contributed to the formation and nucleation of nanocrystallites of aragonite onto the degraded organic matter within the body of the biofilm. Preservation of the aragonite (the oldest known occurrence) was probably due to the combined influence of an organic (kerogenous) matrix and contemporaneous impregnation by hydothermal silica. The JCMB presents all the preservable characteristics of modern photosynthesising microbial mats. It was constructed in the photic zone; it has a laminated, vertically structured architecture including trapped detrital particles; it stabilised the underlying sediment surface; and it was calcified *in situ* by primary aragonite, probably in association with sulphur reducing bacteria degradation of organic material produced by an anoxygenic photosynthesising primary producer. The -26.7‰ carbon isotope signature is consistent with a photosynthetic metabolism and subsequent heterotrophic degradation of photosynthetic carbon.

ACKNOWLEDGEMENTS

Funding was provided by the CNRS, the GDR-Exobiologie, the ANR-Blanc-ARCHAEMAT, and the NSERC. F.W. and C.D. acknowledge A. Richard for help with HR-SEM/cryoSEM and and D. Jalabert HR-TEM at the University of Orléans.

REFERENCES

Allwood, A.C., Walter, M.R., Kamber, B.S., Burch, I.W., 2006. Stromatolite reef from the Early Archaean era of Australia. Nature, 441, 714-719.

Allwood, A.C., Grotzinger, J.P., Knoll, A.H., Burch, I.W., Anderson, M.S., Coleman, M.L., Kanik, I., 2009. Controls on development and diversity of Early Archean stromatolites. Proceedings of the National Academy of Sciences, 106, 9548-9555.

Altermann, W., Schopf, J.W., 1995. Microfossils from the Neoarchaean Campbell Group, Griqualand West Sequence of the Transvaal Supergroup, and their palaeoenvironmental and evolutionary implications. Precambrian Research, 75, 65-90.

Arning, E.T., Birgel, D., Schulz-Vogt, H.N., Holmkvist, L., Jørgensen, B.B., Larsson, A., Peckmann, J., 2008. Lipid biomarker patterns of phosphogenic sediments from upwelling regions. Geomicrobiol. J., 25, 69-82.

Barbieri, R., Cavalazzi, B., 2005. Microbial fabrics from Neogene cold seep carbonates, Northern Apeninne, Italy. Palaeogeography, Palaeoclimatology and Palaeoecology, 227, 143-155.

Banerjee, N.R., Furnes, H., Muehlenbachs, K., Staudigel, H., de Wit, M., 2006. Preservation of 3.4-3.5 Ga microbial biomarkers in pillow lavas and hyaloclastites from the Barberton Greenstone Belt, South Africa. Earth Planetary Science Letters, 241, 707-722.

Berndt, M.E., Seyfried, W.E., 1999. Rates of aragonite conversion to calcite in dilute aqueous fluids at 50-100°C: Experimental calibration using Ca-isotope attenuation. Geochimica et Cosmochimica Acta, 63, 373-381.

Berner, R.A., 1971. Principles of Chemical Sedimentology, McGrawHill, New York.

Bischoff, J.L., Fyfe, W.S., 1968. Catalysis, inhibition and calcite-aragonite problem. I. The calcite aragonite transformation. American Journal of Science, 226, 65-79.

Brasier, M.D., Green, O.R., Jephcoat, A.P., Kleppe, A.K., Van Kranendonk, M.J., Lindsay, J.F., Steele, A., Grassineau, N.V., 2002. Questioning the evidence for Earth's oldest fossils. Nature, 416, 76-81.

Brocks J.J., Logan, G.A., Buick, R., Summons, R.E., 1999. Archean molecular fossils and the early rise of eukaryotes. Science, 285, 1033-1036.

Buick, R., 1992. The antiquity of oxygenic photosynthesis: evidence from stromatolites in sulphate-deficient Archaean lakes. Science, 255, 74-77.

Byerly G.R., Walsh, M.M., Lowe, D.L., 1986. Stromatolites from the 3300-3500 Myr Swaziland Supergroup, Barberton Mountain Land, South Africa, Nature 319, 489-491

Canfield, D.E., Habicht, H.S., Thamdrup, B., 2000. The Archean sulfur cycle and the early history of atmospheric oxygen. Science, 288, 658-661.

Cady, S.L., Farmer, J.D., 1996. Fossilization processes in thermal siliceous springs: trends in preservation along the thermal gradient. In: Evolution of hydrothermal ecosystems on Earth (and Mars?). In: Bock, G.R., Goodie, J.A. (Eds.), Wiley, Chichester, pp 150-173.

Chafetz, H.S., Wu, Z., Lapen, TJ., Milliken, K.L., 2008, Geochemistry of preserved Permian aragonitic cements in the tepees of the Guadalupe Mountains, West Texas and New Mexico. Journal of Sedimentary Research, 78, 187-198.

Défarge, C., 2011. Organomineralization. In: Reitner, J., Thiel, V. (Eds.), Encyclopedia of Geobiology, Springer, Heidelberg, in press.

Défarge, C., Trichet, J., Coute, A., 1994. On the appearance of cyanobacterial calcification in modern stromatolites. Sedimentary Geology, 94, 11-19

Défarge, C., Trichet, J., Jaunet, A.M., Robert, M., Tribble, J., Sansone, F.J., 1996. Texture of microbial sediments revealed by cryo-scanning electron microscopy. Journal of Sedimentary Research, 66, 935-947.

Dunlop, J.S.R., Muir, M.D., Milne, V.A., Groves, D.I., 1978. A new microfossil assemblage from the archeaen of Western Australia. Nature, 274, 676-678.

Dupraz, C., Reid, R.P., Braissant, O., Decho, A.W., Norman, R.S., Visscher, P.T., 2009. Processes of carbonate precipitation in modern microbial mats. Earth-Science Reviews, 96, 141-162.

Dziggel, A., Stevens, G., Poujol, M., Anhaesser, C.R., Armstrong, R.A., 2002. Mettamorphism of the granite-greenstone terrane south of the Barberton greenstone belt, South Africa: an insight into the tectono-thermal evolution of the ‘lower’ portions of the Onverwacht Group. Precambrain Research, 114, 221-247.

Fagerbakke, K.L., Heldal, M., Norland, S., 1996. Content of carbon, nitrogen, oxygen, sulfur and phosphorus in native aquatic and cultured bacteria. Aquatic Microbial Ecology, 10, 15-27.

Garcia-Pichel, F., Mechling, M., Castenholz, R.W., 1994. Diel migrations of microorganisms within a benthic, hypersaline mat community. Applied and Environmental Microbiology, 60, 1500-1511.

Habicht1, K.S., Gade, M., Thamdrup, B., Berg, P., Canfield, D.E., 2002. Calibration of sulfate levels in the Archean ocean. Science, 298, 2372-2374.

Hofmann, A., Bolhar, R., 2007. The origin of carbonaceous cherts in the Barberton greenstone belt and their significance for the study of early life in mid-Archaean rocks. Astrobiology, 7, 355-388.

Hofmann, A., Harris, C., 2008. Stratiform alteration zones in the Barberton greenstone belt: a window into subseafloor processes 3.5–3.3 Ga ago. Chemical Geology, 257, 224-242.

Hofmann, H. J., 1976. Precambrian microflora, Belcher Islands, Canada: Significance and systematics. Journal of Paleontology, 50, 1040-1073.

Hofmann, H.J., Grey, K., Hickman, A.H., and Thorpe, R.I., 1999. Origin of 3.45 Ga coniform stromatolites in Warrawoona Group, Western Australia. Geological Society of America Bulletin, 111, 1256-1262.

Jacobsen, C., Flynn, G., Wirick, S., Zimba, C., 2000. Soft x-ray spectroscopy from image sequences with sub-100 nm spatial resolution. Journal of Microscopy, 197, 173-184.

Jones, B., Renaut, R.W., Rosen, M.R., 2001. Taphonomy of silicified filamentous microbes in modern geothermal sinters – implications for identification. Palaios, 15, 580-592.

Kasting, J.F., 1993. Earth's early atmosphere. Science, 259, 920-926.

Kawano, J., Shimobayashi, N., Miyake, A., Kitamura, M., 2009. Precipitation diagram of calcium carbonate polymorphs: its construction and significance. Journal of Physics-Condensed Matter, 21, 425102.

Knoll, A.H., 1985. Exceptional preservation of photosynthetic organisms in silicified carbonates and silicified peats. Philosophical Transactions of the Royal Society, London 311B, 111-122.

Konhauser, K.O., Phoenix, V.R., Bottrell, S.H., Adams, D.G., Head, I.M., 2001. Microbial-silica interactions in Icelandic hot spring sinter: possible analogues for Precambrian siliceous stromatolites. Sedimentology, 48, 415-433.

Larkin, J., Henk, M.C., Aharon, P., 1994. *Beggiatoa* in microbial mats at hydrocarbon vents in the Gulf of Mexico and Warm Mineral Springs, Florida. Geo-marine Letters, 14, 97-103.

Last, W.M., 1994. Deep-water evaporite mineral formation in lakes of Western Canada. Sedimentology and geochemistry of modern and ancient saline lakes. SEPM Special Publication, 50, 51-59.

Lekstrom, M., McLachlan, M.A., Husain, S., McComb, D.W., Shollock, B.A., 2008. Using the *in situ* lift-out technique to prepare TEM specimens on a single-beam FIB instrument. Journal of Physics: Conference Series 126, 1-4.

Lemelle, L. Labrot, P., Salomé, M., Simionovici, A., Viso, M., Westall, F., 2008. In situ imaging of organic sulfur in 700-800 My-old Neoproterozoic microfossils by X-ray spectromicroscopy at the S K-edge. Organic Geochemistry, 39, 188-202.

Lepot, K., Benzerara, K., Brown, G., Philippot, P., 2008. Microbially influenced formation of 2,724-million-year-old stromatrolites. Nature Geoscience, 1, 118-121.

Lowe, D.R., 1980. Stromatolites 3,400-Myr old from the Archean of Western Australia. Nature, 284, 441-443.

Lowe, D.R., 1983. Restricted shallow water sedimentation of early Archean stromatolitic and evaporitic strata of the Strelley Pool Chert, Pilbara Block, Western Australia. Precambrian Research, 19, 239-283.

Lowe, D.R., 1994. Abiological origin of described stromatolites older than 3.2 Ga. Geology, 22, 287-390.

Lowenstein, T.K., Hardie, L.A., 1985. Criteria for the recognition of salt-pan evaporites. Sedimentology, 32, 627-644.

Mojzsis, S.J., Arrhenius, G., McKeegan, K.D., Harrison, T.M., Nutman, A.P., Friend, C.R.L., 1996. Evidence for life on Earth before 3800 million years ago. Nature, 384, 55-59.

Knoffke, N., 2009. The criteria for the biogeneicity of microbially induced sedimentary structures (MISS) in Archean and younger, sandy deposits. Earth-Science Reviews, 96, 173-180.

Orange, F., Westall, F., Disnar, J.-R., Prieur, D., Bienvenu, N., Le Romancer, M., Défarge, Ch. 2009. Experimental silicification of the extremophilic Archaea *Pyroccus abyssi* and *Methanocaldococcus jannaschii*. Applications in the search for evidence of life in early Earth and extraterrestrial rocks. Geobiology, 7, 403-418.

Pentecost, AL., 2005. Travertines. Springer, Berlin. 445pp.

Power, I.M., Wilson, S.A., Thom, J. Dipple, G., Southam, G., 2009. The hydromagnesite playas of Atlin, British Columbia: A biogeochemical model for CO_2 sequestration. Chemical Geology 260, 286-300.

Rasmussen, B., Fletcher, I.R., Brocks, J.J., Kilburn, M.R., 2008. Reassessing the first appearance of eukaryotes and cyanobacteria. Nature, 455, 1101-1104.

Reimers, C., Kastner, M., Garrison, R.E., 1990. The role of bacterial mats in phosphate mineralization with particular reference to the Monterey Formation. In Phosphate Deposits of

the World. Volume 3: Neogene to Modern Phosphorites, edited by W.C. Burnett and S.R. Riggs, Cambridge University Press, Cambridge, pp 300-311.

Rosing M.T., 1999. ^{13}C depleted carbon microparticles in >3700 Ma seafloor sedimentary rocks from West Greenland. Science, 283, 674–676.

SACS (South African Committee for Stratigraphy), 1980. Stratigraphy of South Africa, Part 1: Lithostratigraphy of the republic of South Africa, Soutwest Africa/Namibia and the Republics of Bophuthatswana, Transkei, and Venda. Geol. Survey of South Africa, Handbook, 8,690 p.

Schidlowski, M., 1988. A 3800 million-year isotopic record of life from carbon in sedimentary rocks. Nature, 333, 313-318.

Schidlowski, M., 2001. Carbon isotopes as biogeochemical recorders of life over 3.8 Ga of Earth history: Evolution of a concept. Precambrian Research, 106, 117-134.

Schopf, J.W., 1993. Microfossils of the Early Archean Apex Chert: New evidence of the antiquity of life. Science, 260, 640-646.

Schopf, J.W., and Walter, M.R., 1983. Archean microfossils: new evidence of ancient microbes. In Earth's earliest biosphere: its origin and evolution, ed. J.W. Schopf. Princeton: Princeton University Press, pp. 214-239.

Schulz, H.N., Brinkhoff, T., Ferdelman, T., Marine, M.H., Teske, A., Jørgensen, B.B., 1999. Dense populations of a giant sulfur bacterium in Namibian shelf sediments. Science, 284, 493-495.

Schulz, H.N., Strotmann, B., Gallardo, V.A., Jørgensen, B.B., 2000. Population study of the filamentous sulfur bacteria *Thioploca* spp. off the Bay of Concepcion, Chile. Marine Ecology Progress Series, 200, 117-126.

Summons, R.E., 1993. A review of fundamental aspects of organic matter formation, preservation and composition. In: Engel, M.A., Macko, S.A. (Eds.), Organic Geochemistry, Principles and Applications. Plenum Press, New York, pp. 3-21

Summons, L.L. Jahnke, J.M. Hope, G.A. Logan, N., 1999. Molecular fossils for cyanobacteria recording a geological history of oxygenic photosynthesis. Nature, 400, 554-557.

Susini, J., Salome, M., Fayard, B., Ortega, R., Kaulich, B., 2002. The scanning X-ray microprobe at the ESRF by X-ray microscopy beamline. Surface Review and Letters, 9, 203-211.

Tice, M.M., 2009. Environmental controls on photosynthetic microbial mat distribution and morphogenesis on a 3.42Ga clastic-starved platform. Astrobiology, 9, 989-1000.

Tice, M., Lowe D.R., 2004. Photosynthetic microbial mats in the 3,416-Myr-old ocean: Nature, 431, 549–552

Tice, M., Lowe, D.R., 2006. The origin of carbonaceous matter in pre-3.0 Ga greenstone terrains: a review and new evidence from the 3.42 Ga Buck Reef Chert. Earth-Science Reviews 76, 259-300.

van Zuilen, M.A., Lepland, A., Arrhenius, G., 2002. Reassessing the evidence for the earliest traces of life. Nature, 418, 627-630.

Visscher, P.T., Stolz, J., 2005. Microbial communities as biogeochemical reactors. Paleogeography, Paleoclimatology and Paleoecology, 119, 87-100

Wacey, D., 2010. Stromatolites in the 3400 Ma Strelley Pool Formation, Western Australia: examining biogenicity from the macro- to the nano-scale. Astrobiology, 10, 381-395.

Walsh, M.M., 1992. Microfossils and possible microfossils from the Early Archean Onverwacht Group, Barberton Mountain Land, South Africa. Precambrian Research, 54, 271-293.

Walter, M. R., Ed., 1976 - Stromatolites. Elsevier Scientific Publishing Co., 790

Westall, F., 1997. The influence of cell wall composition on the fossilisation of bacteria and the implications for the search for early life forms. In C. B. Cosmovici, S. Bowyer, and D. Werthimer (Eds.) Astronomical and Biochemical Origins and the Search for Life in the Universe, Editrici Compositori, Bologna, 491-504.

Westall, F., 2004. Early life on Earth : the ancient fossil record. In. Ehrenfreund et al., (Eds.) Astrobiology: future perspectives. Kluwer (Doordrecht, Netherlands), pp. 287-316.

Westall, F., 2010. Early life: Nature, distribution, and evolution. In Origins of life, an astrobiology perspective, eds. Gargaud, M. et al. (Cambridge University Press),391-413.

Westall, F. de Witt, M.J., Dann, J., van der Gaast, S., de Ronde, C., Gerneke, D., 2001. Early Archean fossil bacteria and biofilms in hydrothermally-influenced sediments from the Barberton greenstone belt, South Africa. Precambrian Research, 106, 93-116.

Westall, F. de Ronde, C.E.J., Southam, G., Grassineau, N., Colas, M., Cockell, C. Lammer, H., 2006. Implications of a 3.472–3.333 Gyr-old subaerial microbial mat from the Barberton greenstone belt, South Africa for the UV environmental conditions on the early Earth. Philosophical Transactions of the Royal Society B., 361, 1857-1875.

Westall, F., Foucher, F. and Cavalazzi, B., de Vries, S.T., Nijman, W., Pearson, V., Watson, J., Verchovsky, A., Wright, I., Rouzaud, J-N., Marchesini, D., Anne, S., 2010. Volcaniclastic habitats for early life on Earth and Mars: A case study from 3.5 Ga-old rocks from the Pilbara, Australia. Planetary and Space Science, doi:10.1016/j.pss.2010.09.006, in press.

FIGURE CAPTIONS

Figure 1. The Josefsdal Chert.

(A) Detailed geological map of Josefsdal Chert study area showing the sample site (in dashed square). **(B)** Stratigraphical column of the Josefsdal Farm locality (after Hofmann and Bohlar, 2007) showing the JC outcrops that are mapped as a black and white banded chert situated near the top of the Kromberg Forbiofilmion.

Figure 2. Location of FIB sections in the Josefsdal Chert Microbial Biofilm (JCMB).

(A) Plan view of one of the portions of the JCMB exposed on a bedding plane of the Josefsdal Chert showing the location of some of the FIB sections (box) before the sections were made. Solid arrows indicate flow orientation of the filamentous biofilm. **(B**) Detail showing the section trenches. Dashed arrowsshow locations of FIB sections for SEM and TEM observation.

Figure 3. Backscatter SEM micrographs of FIB slices cut vertically through the Josefsdal Chert showing its structural and compositional heterogeneity.

(A). The JSMB sits on re-crystallised silicified sediment (Qtz) (boundary marked by the dashed line) but has partially lifted off the sedimentary substrate to the right where the bright phase lining the basal gap is gallium coming from the Ga milling. The biofilm consists of a thick layer of kerogen (**ke**). **Cal -** a calcite grain (arrow) related to the precipitation of evaporite minerals on top of the biofilm. The body of the biofiklm beneath the kerogen is partly calcified (**Cb**). A 2 µm thick coat of Pt (**Pt**) was deposited on top of this part of the biofilm in order to protect it during FIB milling. **(B)** The biofilm in this FIB slice is characterised by evaporite minerals (**Ev**) embedded in its surface (cf. carbonate grain in the

top of the biofilm in Figure 4a); a thin kerogen (**Ke**) layer at the top of the biofilm (above the dotted line); the main body of the biofilm is calcified (**Cb**) and contains "floating "grains of quartz (**Qtz**); a thick scalloped layer of silica (**Si**) at the base of the biofilm (which has lifted off the substrate in this location).

Figure 4. Elemental composition of the carbonate phases in the JCMB.
Elemental mapping of the FIB section shown in Figure 4a (µXRF for Ca, Cr, Fe; EDX for Mg) showing that the calcified part of the biofilm contains Ca, Mg, Cr and Fe.

Figure 5. Nanostructure of the JCMB.
(A) Dark field STEM micrograph of a 90 nm thick FIB section showing a small portion of alveolar kerogen at the top (left) of the biofilm, the main body of which has a granular texture. Note that the biofilm has slightly lifted from the underlying silicified sediment in this section (bottom left). Boxed areas indicate locations of details shown in Supplementary Figure 3. **(B)** HR-TEM micrograph of the kerogen showing small stacks of 1 nm long fringes outlined by the dotted lines that correspond to locally piled up polyarobiofilmic structures. Their presence indicates that the kerogen is relatively biofilmure.

Figure 6 Nanostructure of the calcified part of the JCMB. **(A)** TEM micrograph of a part of the calcified biofilm showing the contact (dotted line) between the calcified part and the kerogen. The diffractogram (inset) shows the distribution of the crystal planes of aragonite. The boxed area shows the area analysed by HR-TEM in (B). **(B)** HR-TEM view of the calcified area in which individual nanocrystals 5-10 nm in size can be seen. The interlayer spacing (0.335 nm) is that of the d_{111} plane of aragonite. The inset is a FFT (Fast Fourrier Transform) view of the distribution of the crystal planes showing different discrete spots,

indicating that the area analysed consists of a number of differently orientatied aragonite crystallites.

Figure 7. NanoSIMS mapping of carbon, nitrogen, and sulphur in the FIB slice shown in Figure 4b.
(A) Backscatter SEM image of the FIB section analysed by NanoSIMS. **(B)** Carbon (as ^{12}C), **(C)** nitrogen (as $^{12}C/^{12}C\ ^{14}N$), **(D)** sulphur (^{32}S). The kerogen-rich layer at the top of the biofilm and the small kerogen-rich area in the center of the biofilm are clearly highlighted by the N, and S maps.

Figure 8. µXANES mapping and analysis of sulphur in the FIB slice shown in Figure 4b.
(A) µXANES map of sulphur distribution showing concentrations in the kerogen layer at the top of the biofilm and within the evaporite minerals (pseudomorphed gypsum) embedded in the top of the biofilm. Locations of spot spectral analyses at the S-Kedge: red circle in the kerogen-rich layer at the top of the biofilm and black circle in the calcified part of the biofilm.
(B) µXANES spot spectral analyses at the S-K-edge in the kerogen and carbonate layers. The kerogen layer is characterised by a high peak at 2474 eV representing a heterocyclic organic compound, identified as thiophene (cf. Lemelle et al., 2008). It also contains a small amount of inorganic sulphur in the form of sulphate at 2482.5 eV. The calcified part of the biofilm has a higher sulphate peak but still contains a small amount of thiophene.

Figure 9. NanoSIMS mapping of silica (Si^{28}) in the FIB slice shown in Figures 4b and 7a. (**A**) Backscatter image of the FIB section analysed. (**B**) Silica (Si^{28}) map in the FIB section. The vertical dashed white line shows the location of the profile of Si (**C**).

SUPPLEMENTARY FIGURE CAPTIONS

Supplementary Figure 1. Modern microbial biofilms

(A) Alveolar structure of EPS in a photosynthesizing microbial biofilm, lake Oteaeva-1, Rangiroa atoll. The morphological remains of a cyanobacterial sheath and filament can be recognized in the centre of the image. **(B)** *In situ* calcification in a photosynthesing microbial biofilm. High Mg-calcite (10-17 mol % $MgCO_3$), brownish grey horizontal laminae alternate with carbonaceous dark laminae. The slight birefringence noticeable in the organic layers is due to the organised alveolar structure of the EPS (as in A). Vertical thin-section of resin-indurated sediment in polarized light, lake R2, Rangiroa atoll. The inset shows a cryoSEM micrograph of high-Mg calcite crystals nucleating onto reorganised EPS (lake M3, atoll de Moruroa, Défarge et al., 1996).

Supplementary Figure 2. The Josfsdal Chert and microbial biofilm. **(A)** Hand specimen view of the banded black and white chert in which the Josefsdal Chert Microbial Biofilm (JCMB) occurs. Scale in mm. **(B)** JCMB in plan view on a sediment bedding surface. Note the embedded ~ 200 µm-sized volcanic clasts trapped within the biofilm (small arrows). The large arrows denote the main orientation of the filamentous biofilm.

Supplementary Figure 3. Petrographic thin section view of a microbial biofilm viewed in the Josefsdal Chert. **(A)** Wispy wavy microbial biofilm formed on a sediment surface in the Josefsdal Chert. The laminated biofilm consists of a packet of anastomosing, fine carbonaceous horizons that conformably coat and stabilise the underlying sediment surface. The box shows the area detailed in (B). **(B)** Detail showing the fine wavy carbonaceous layers. The box shows the area detailed in (C). **(C)** Detail showing trapped detrital particles. Thin section micrographs in transmitted light.

Supplementary Figure 4. SEM view of the Josefsdal Chert fracture surface showing several generations of biofilm structures (1, 2) stacked on top of each other and separated by a thin layer of sediment.

Supplementary Figure 5: Raman mineral mapping of a kerogen-rich layer in the Josefsdal Chert, similar to that analysed by ToF-SIMS (Figure 8). **(A)** Micrograph of the kerogen-rich layer (transmitted light). Box indicates zone mapped by Raman. **(B)** Total Raman map showing quartz in orange, anatase in blue, kerogen in green, pyrite in pink, and rutile in red. **(C)** Corresponding Raman spectrum of the kerogen in mapped in (B) indicating relative maturity of the kerogen.

Supplementary Figure 6. ToF-SIMS analysis *in situ* on the carbon-rich layers of the Josefsdal Chert. A number of polyaromatic molecules fragments were detected including $C_7H_7^+$ (tropylium) at 91.05m/z, $C_9H_7^+$ at 115.05 m/z, $C_{10}H_8^+$ (naphthalene) at 128.06 m/z, and $C_{14}H_{10}^+$ (anthracene/phenanthrene) at 178.06 m/z.

Supplementary Figure 7. Nanostructural details of the JCMB. **(A, B).** Details of Figure 5a showing an alveolar texture in the granular part of the biofilm (A) that mimics that in the kerogenous area (B).

Supplementary Figure 8. (A) NEXAFS map showing concentrations of carbon in the kerogen layer at the top of the biofilm and **(B)** spectral peaks at 287.3 eV and 287.4 eV identified as thiophene.

Supplementary Figure 9. Sketch showing sequence of events influencing the JCMB. **(A)** Formation of the biofilms (the stack making up a mat) on a sediment surface by anoxygenic photosynthesisers. **(B)** *In situ* calcification of the mat/biofilms due to degradation by sulphur reducing bacteria of the organic material produced by the photosynthetic primary producers. **(C)** Exposure of the mat/biofilms to dry, evaporitic conditions, encrustation by evaporite minerals and desiccation. Phases (B) and (C) could be simultaneous. **(D)** Permeation and encrustation of the mat/biofilms and the underlying sediment by silica.

Highlights

- *In situ* calcification (aragonite) of a 3.3 Ga microbial biofilm
- Calcification probably due to the activities of a photosynthetic consortium of microorganisms within the biofilm including heterotrophic sulphur reducing bacteria
- Preservation of the metastable carbonate phase by the organic matrix and secondary silicification

Oldest known occurrence of aragonite.

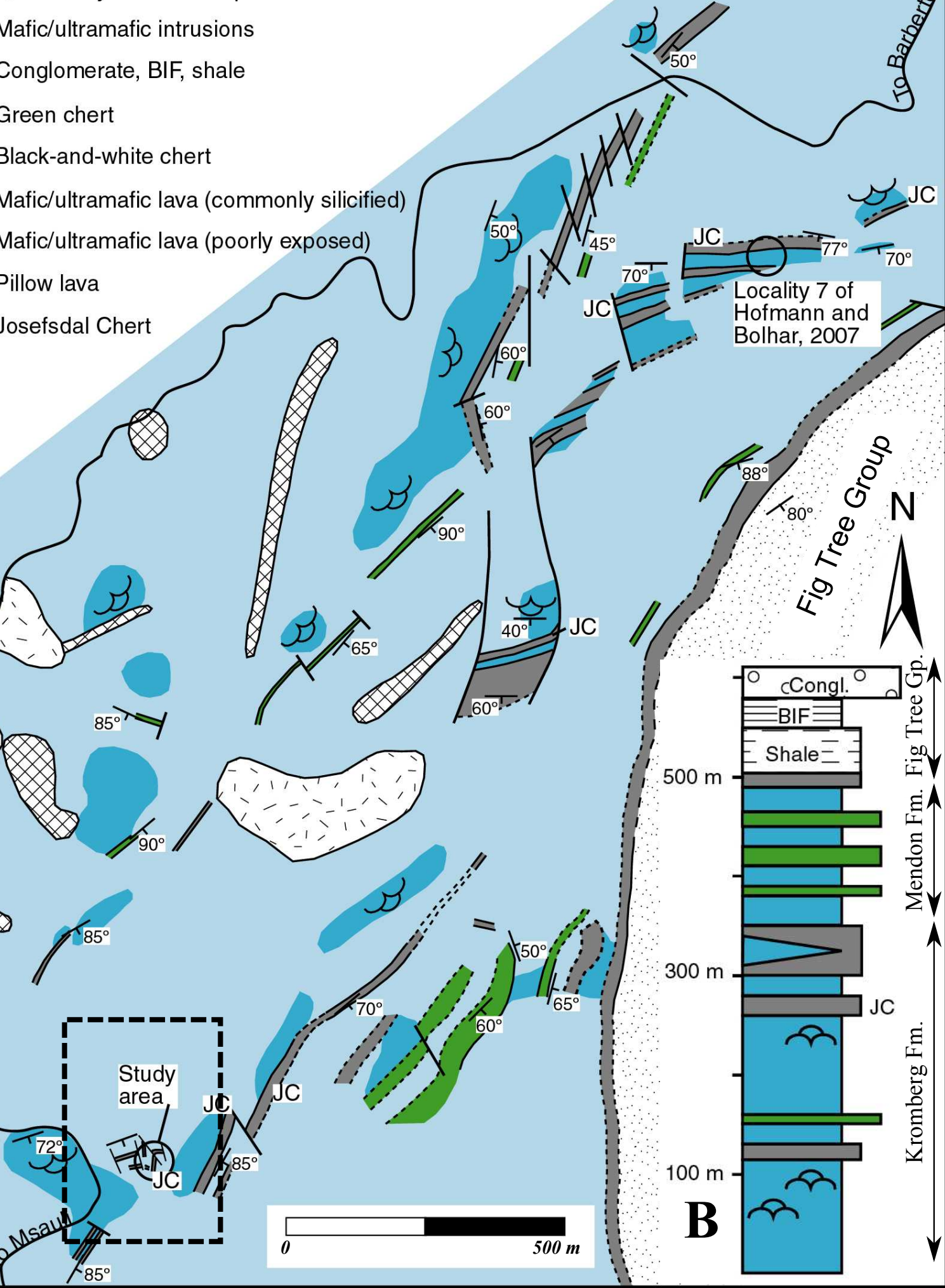
Mafic/ultramafic intrusions
Conglomerate, BIF, shale
Green chert
Black-and-white chert
Mafic/ultramafic lava (commonly silicified)
Mafic/ultramafic lava (poorly exposed)
Pillow lava
Josefsdal Chert
To Barberton
Locality 7 of Hofmann and Bolhar, 2007
Fig Tree Group
N
Study area
JC
50°
45°
77°
70°
60°
90°
88°
80°
40°
65°
85°
72°
Msauli
0
500 m
Congl.
BIF
Shale
500 m
300 m
100 m
Mendon Fm.
Fig Tree Gp.
Kromberg Fm.
B

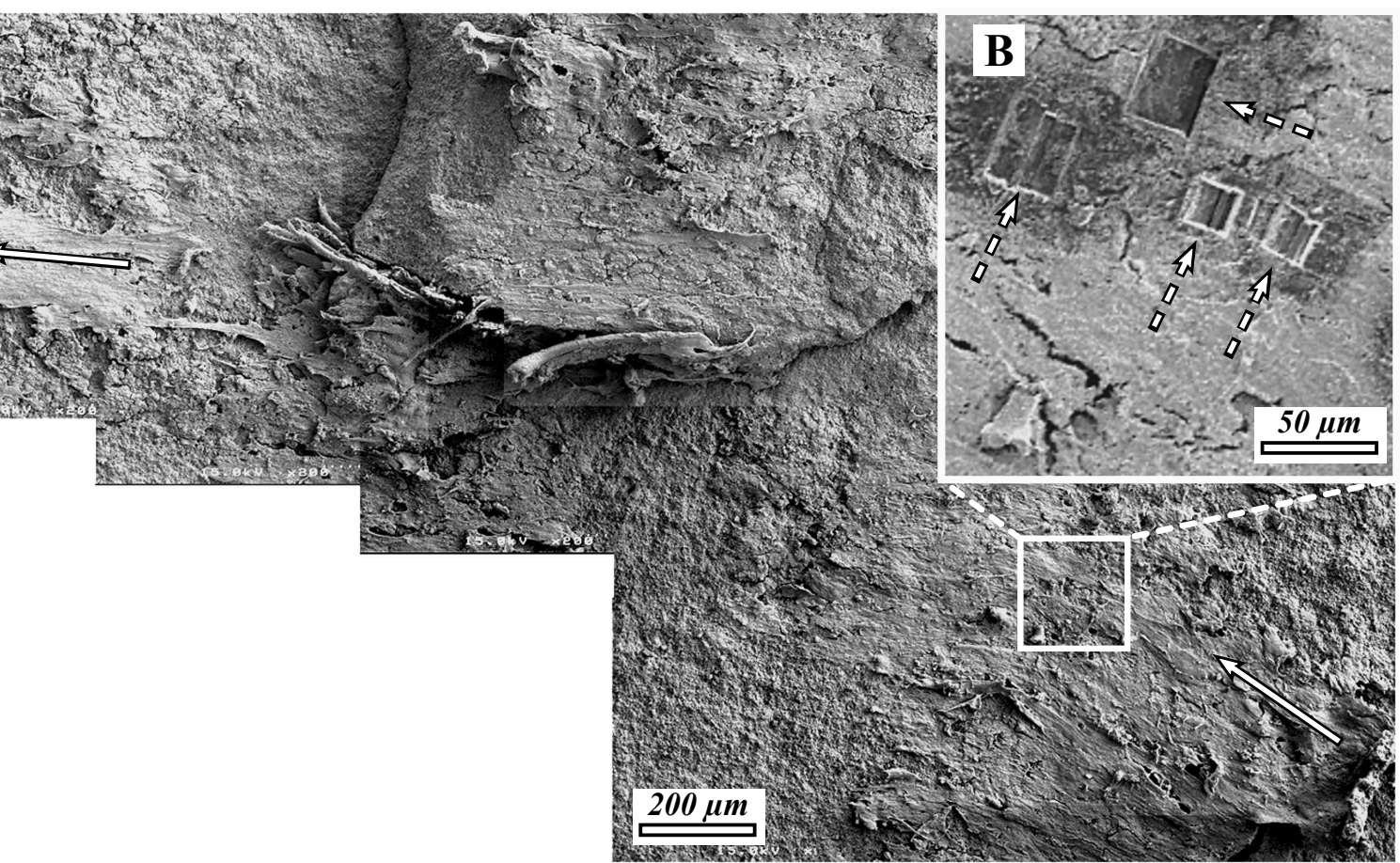
B
50 μm
200 μm

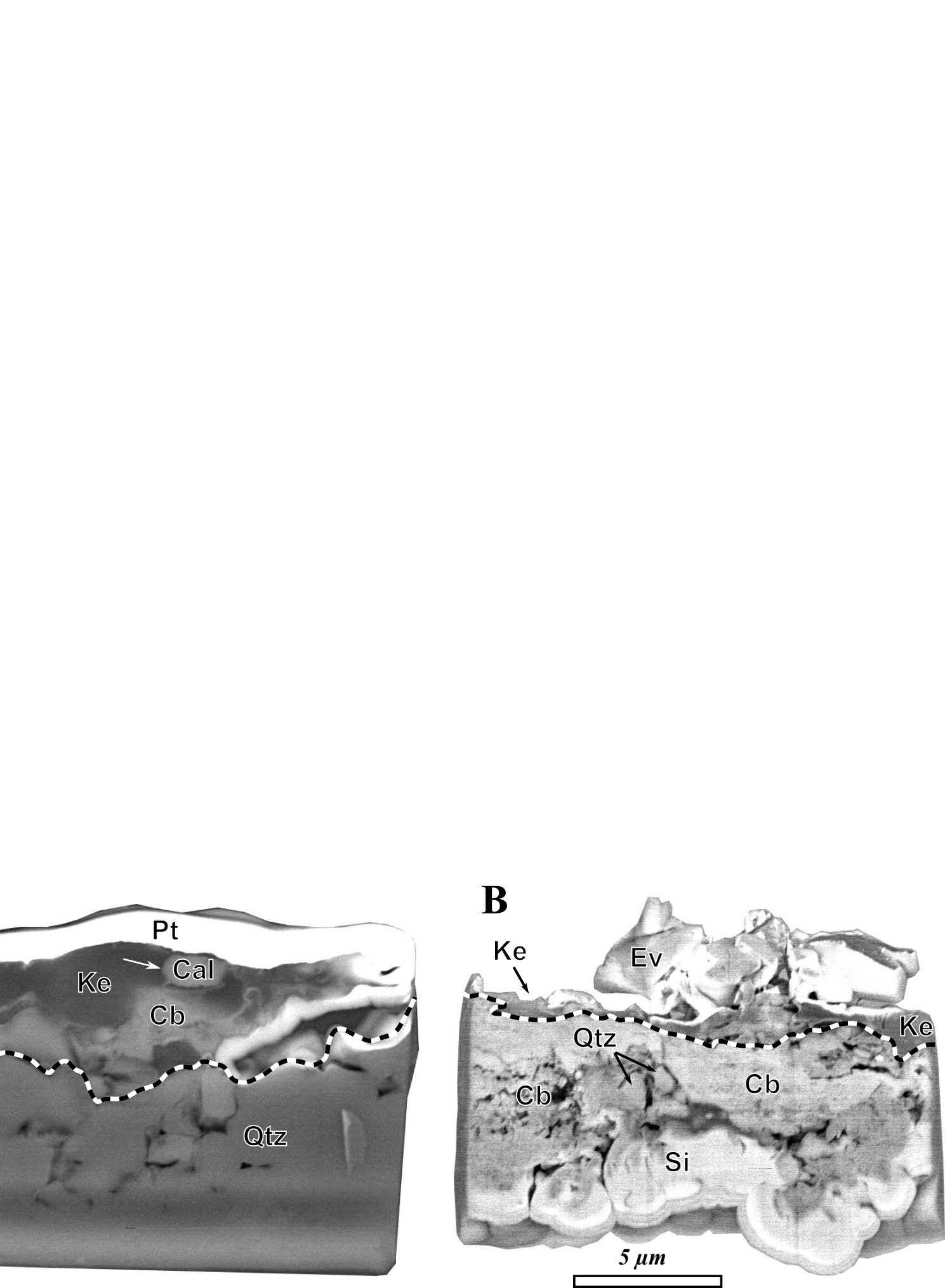
Pt
Cal
Ke
Cb
Qtz
B
Ke
Ev
Ke
Qtz
Cb
Cb
Si
5 μm

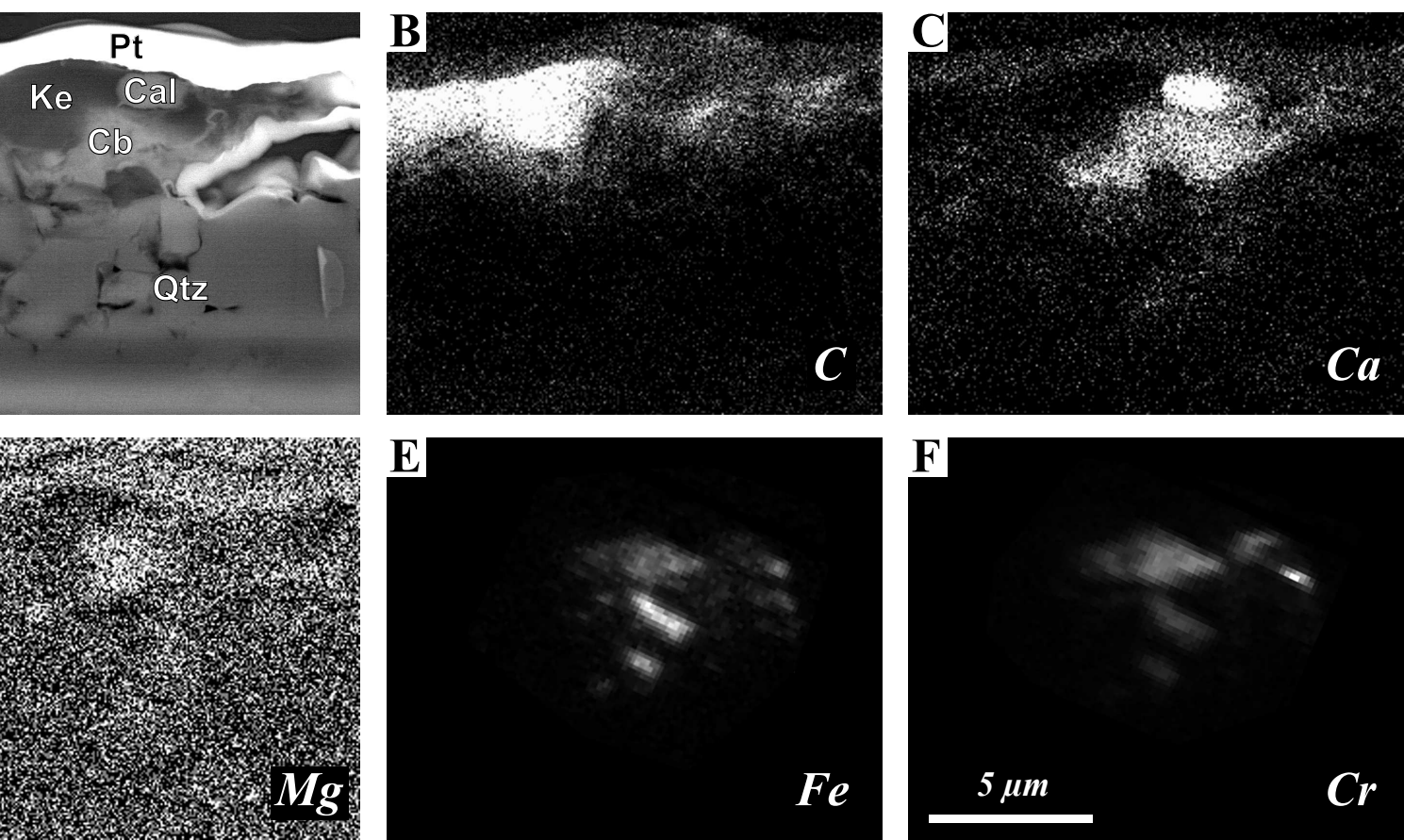
Pt
Ke
Cal
Cb
Qtz
B
C
C
C
Ca
Mg
E
Fe
F
5 μm
Cr

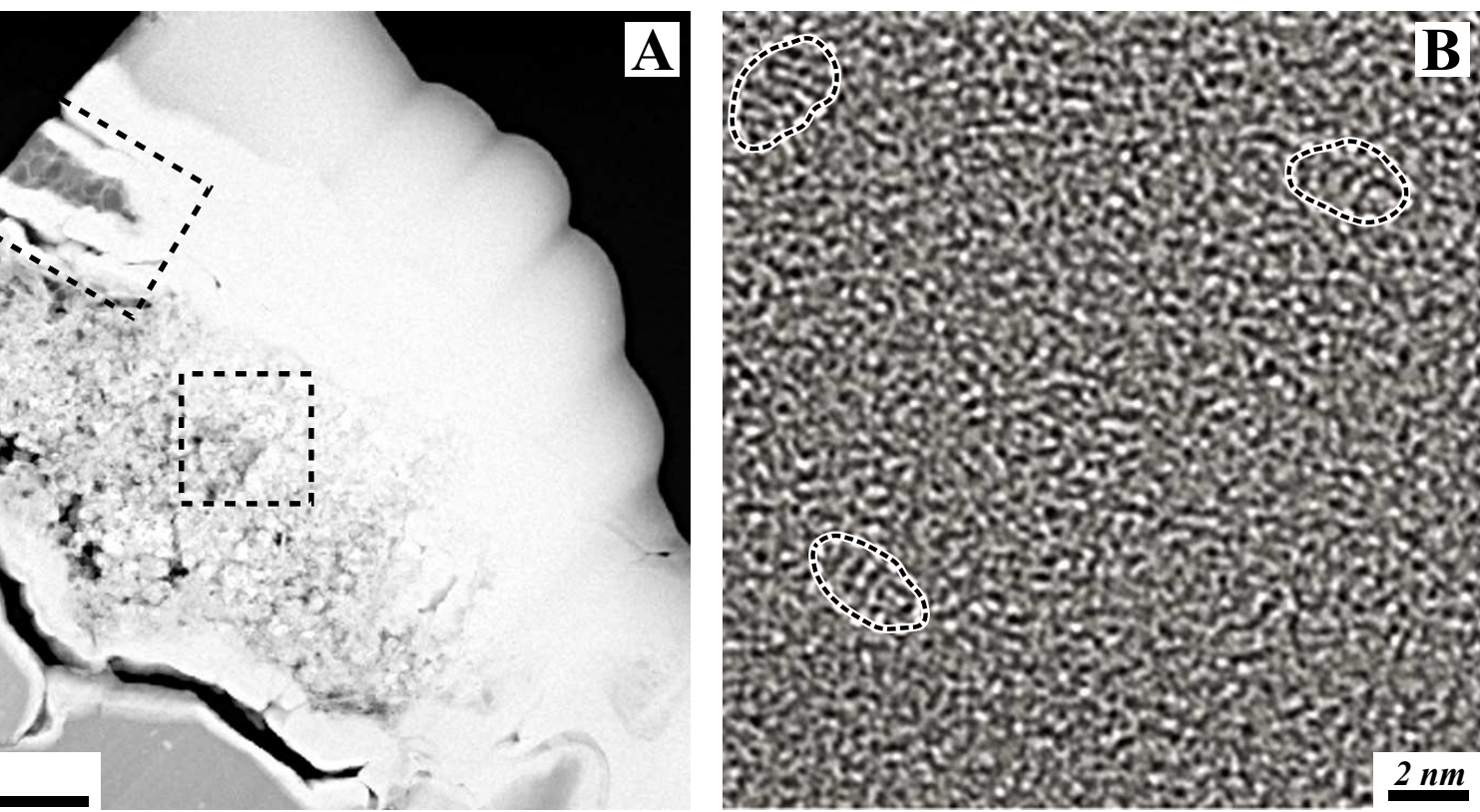
A
B
2 nm

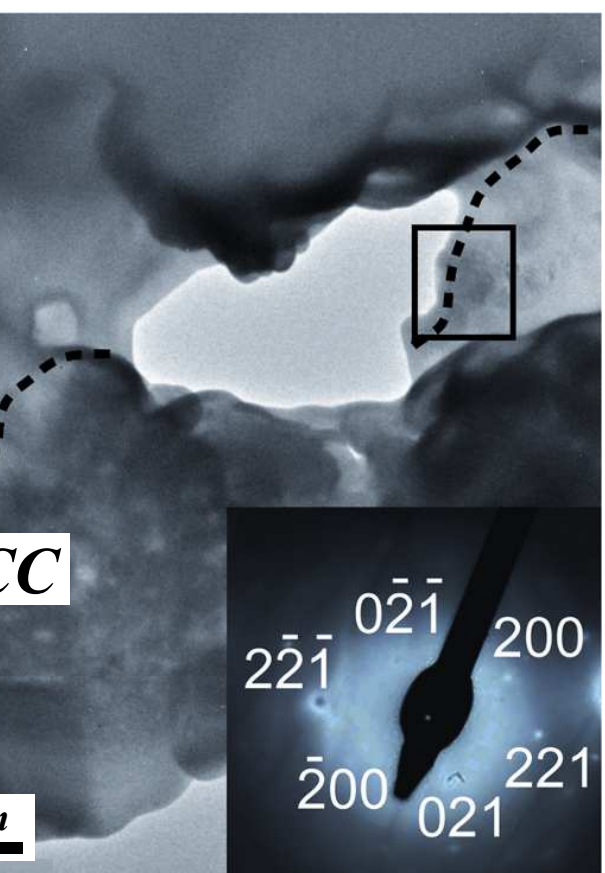
CC
$02\bar{1}\bar{1}$
200
$2\bar{2}\bar{1}\bar{1}$
$\bar{2}00$
221
021

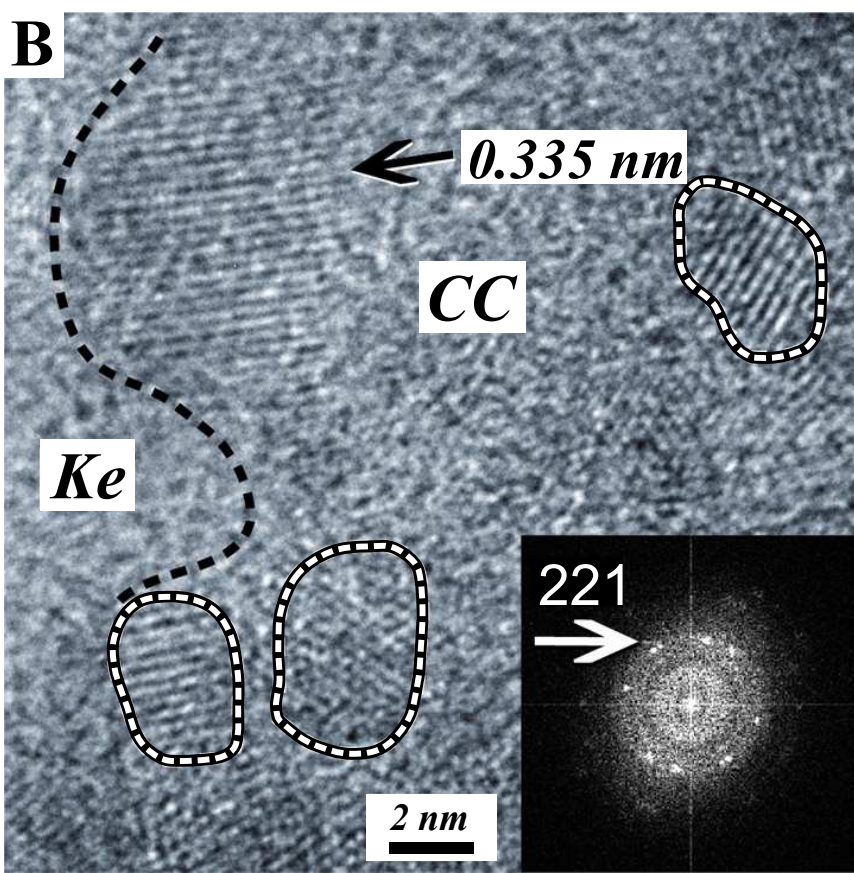
B
0.335 nm
CC
Ke
221
2 nm

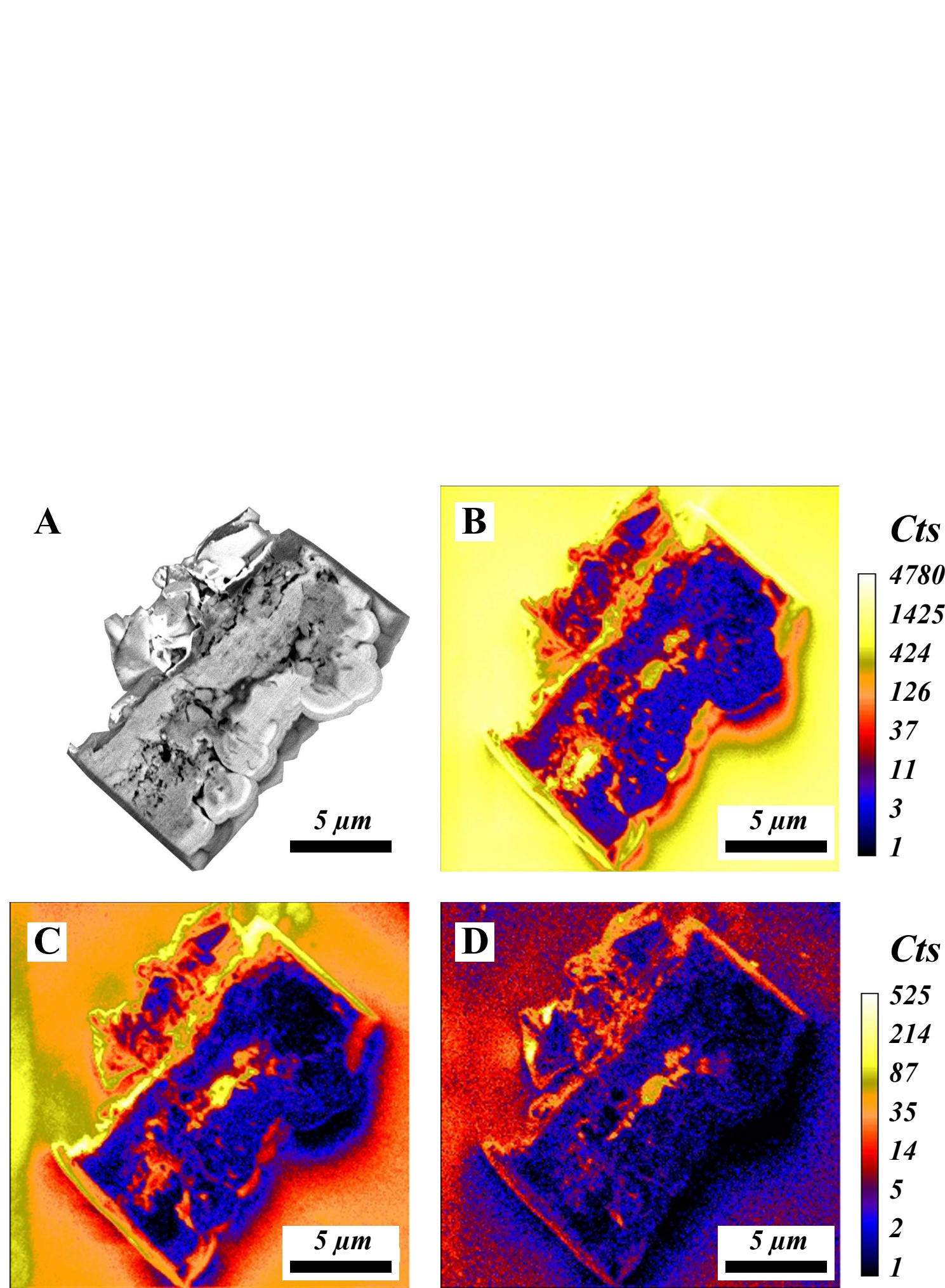
A
5 µm
B
5 µm
Cts
4780
1425
424
126
37
11
3
1
C
5 µm
D
5 µm
Cts
525
214
87
35
14
5
2
1

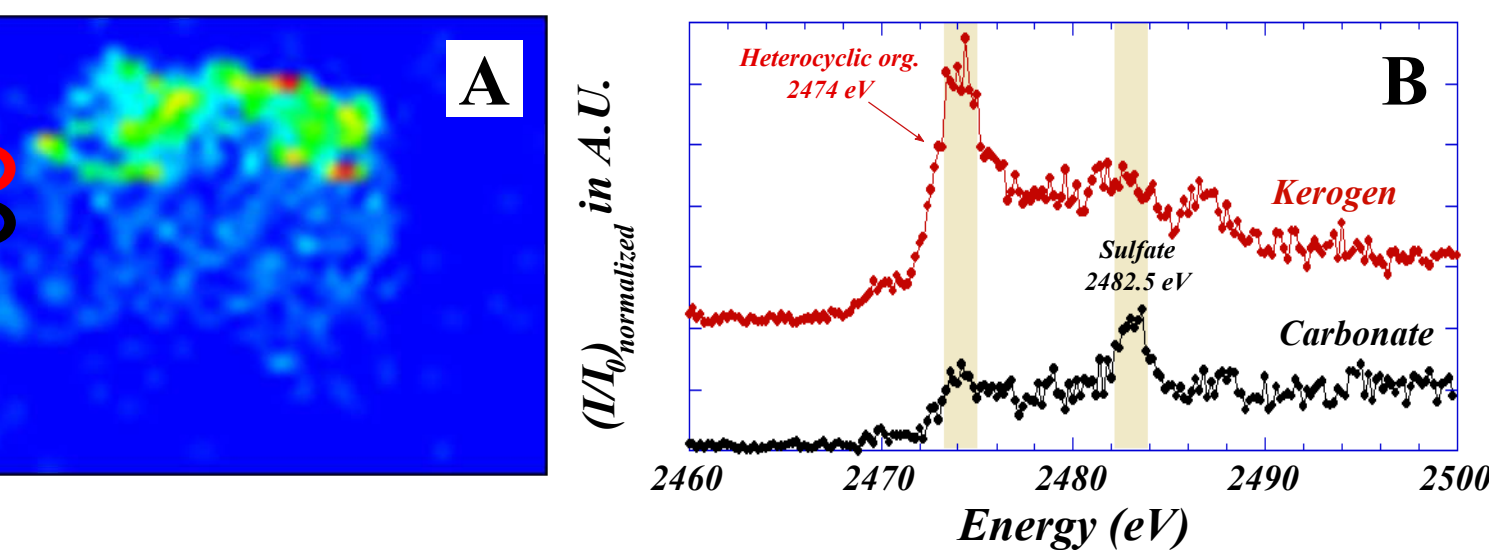
A
B
Heterocyclic org.
2474 eV
Kerogen
Sulfate
2482.5 eV
Carbonate
$(I/I_0)_{normalized}$ in A.U.
2460
2470
2480
2490
2500
Energy (eV)

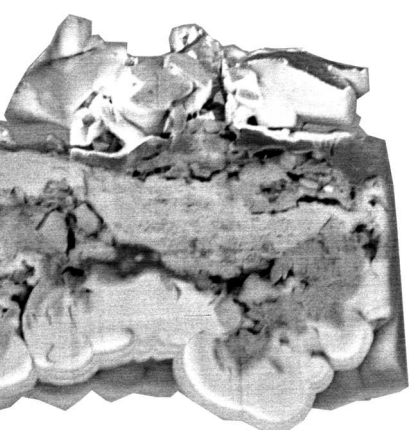
5 µm

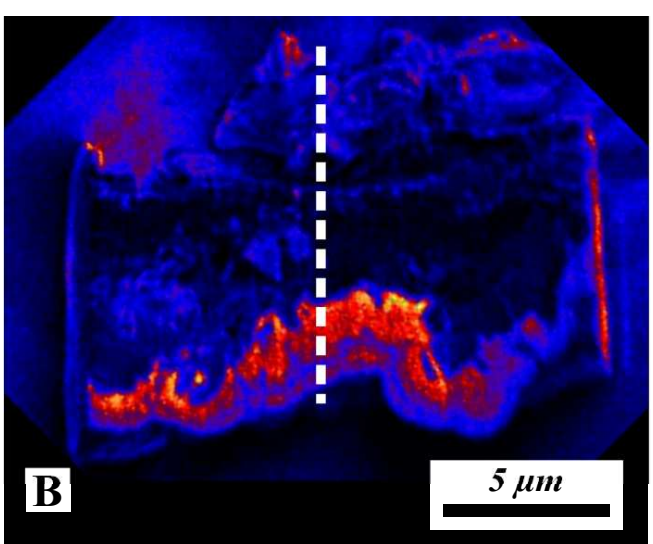
B
5 µm

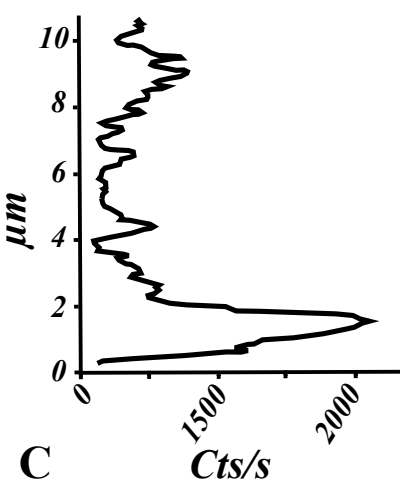
C
µm
10
8
6
4
2
0
0
1500
2000
Cts/s

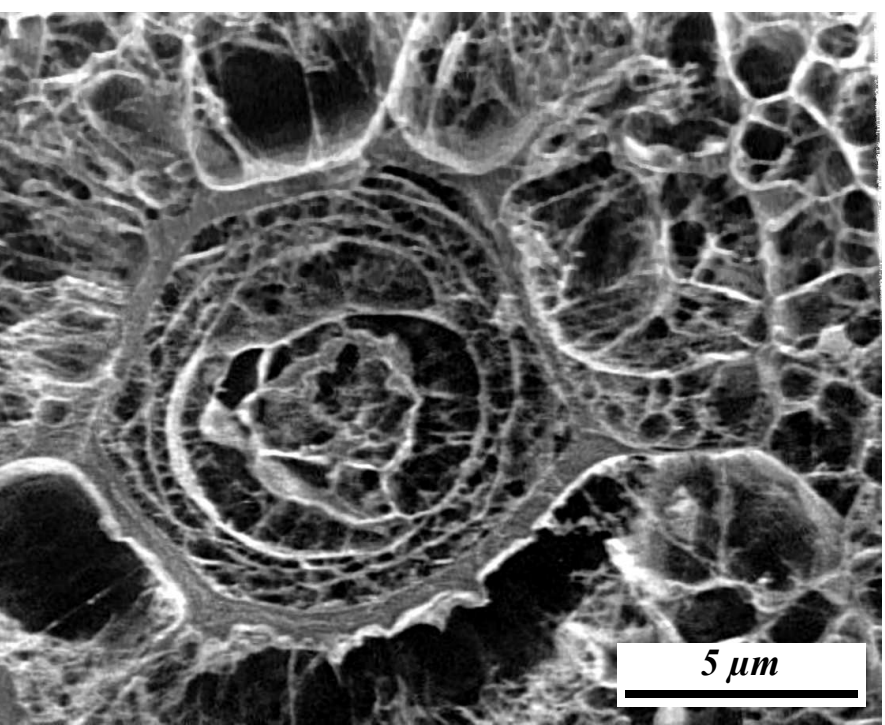
5 µm

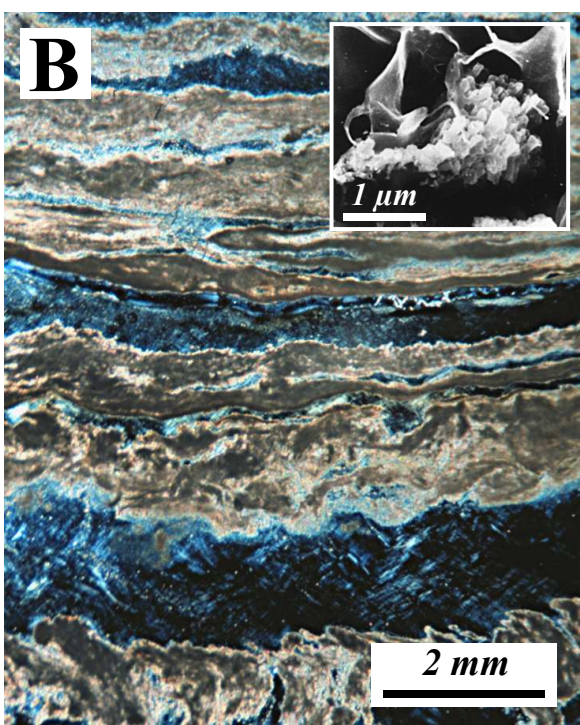
B
1 µm
2 mm

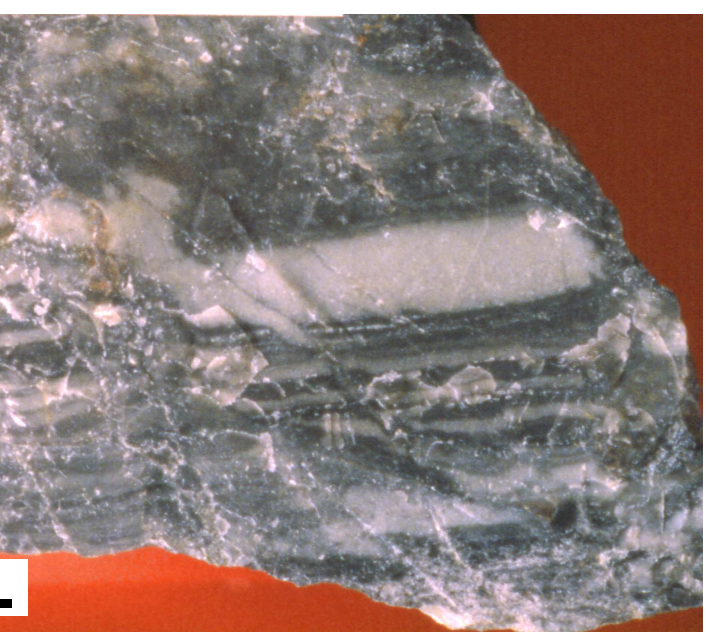

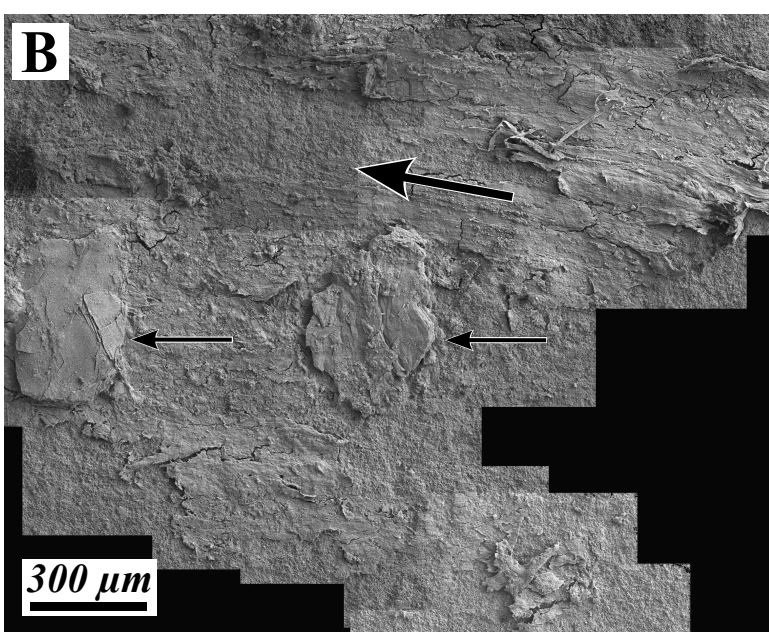
B
300 μm

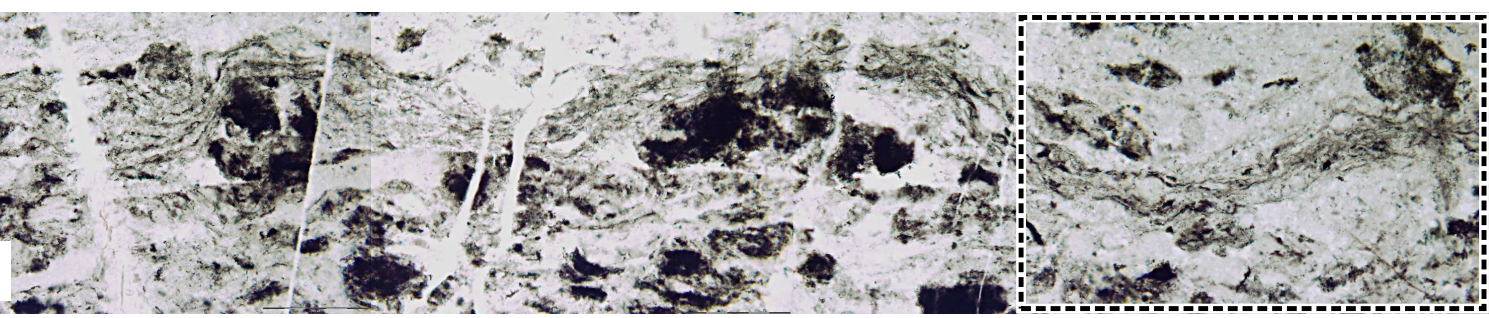

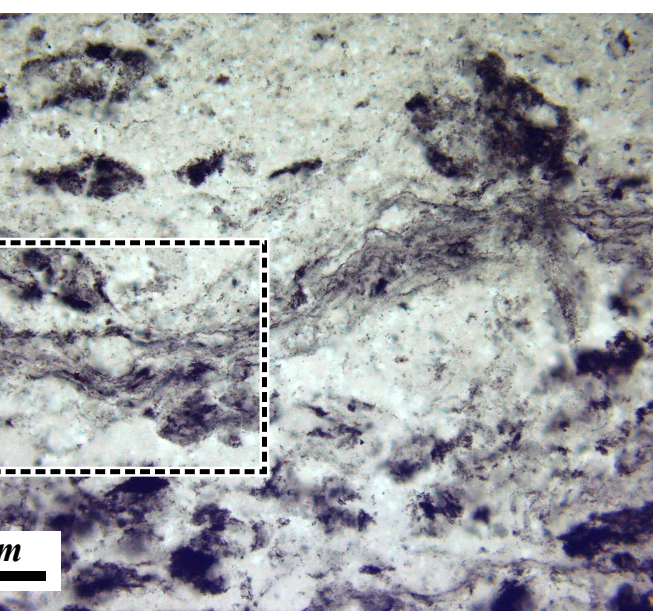

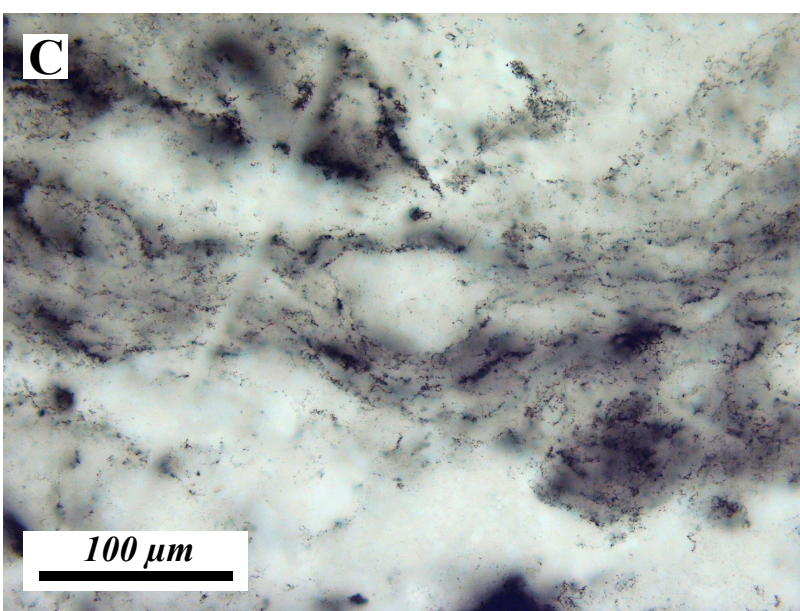
C
100 µm

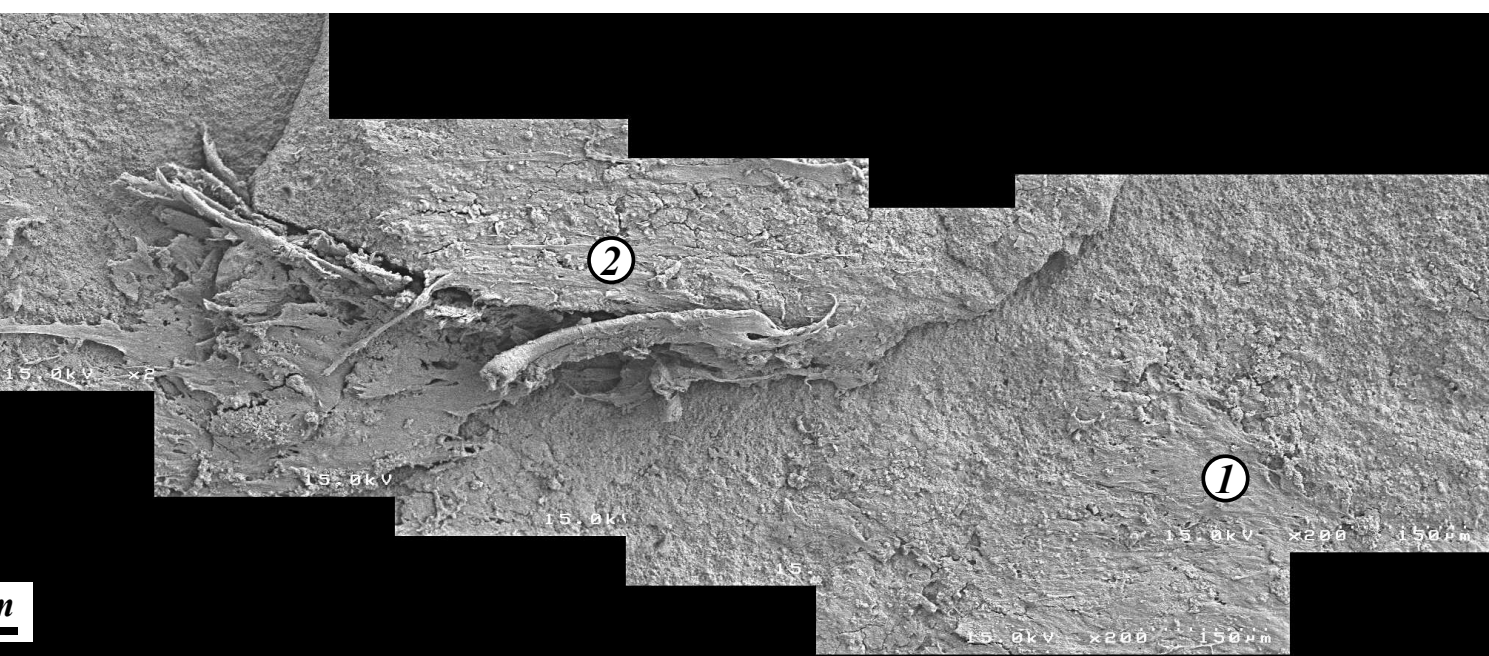
2
15.0kV ×2
15.0kV
15.0k
15.
1
15.0kV ×200 150µm
15.0kV ×200 150µm

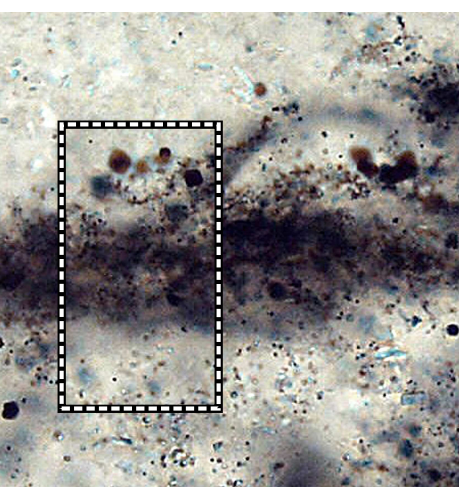

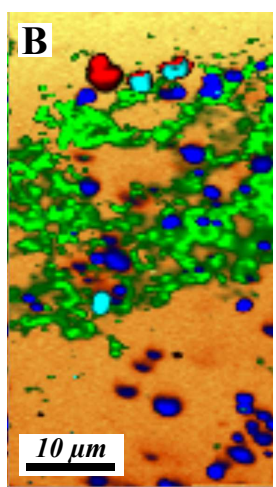
B
10 μm

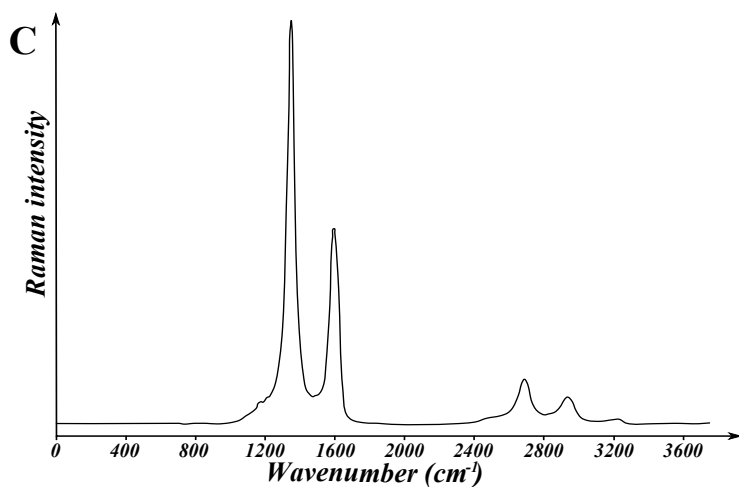
C
Raman intensity
0
400
800
1200
1600
2000
2400
2800
3200
3600
Wavenumber (cm-1)

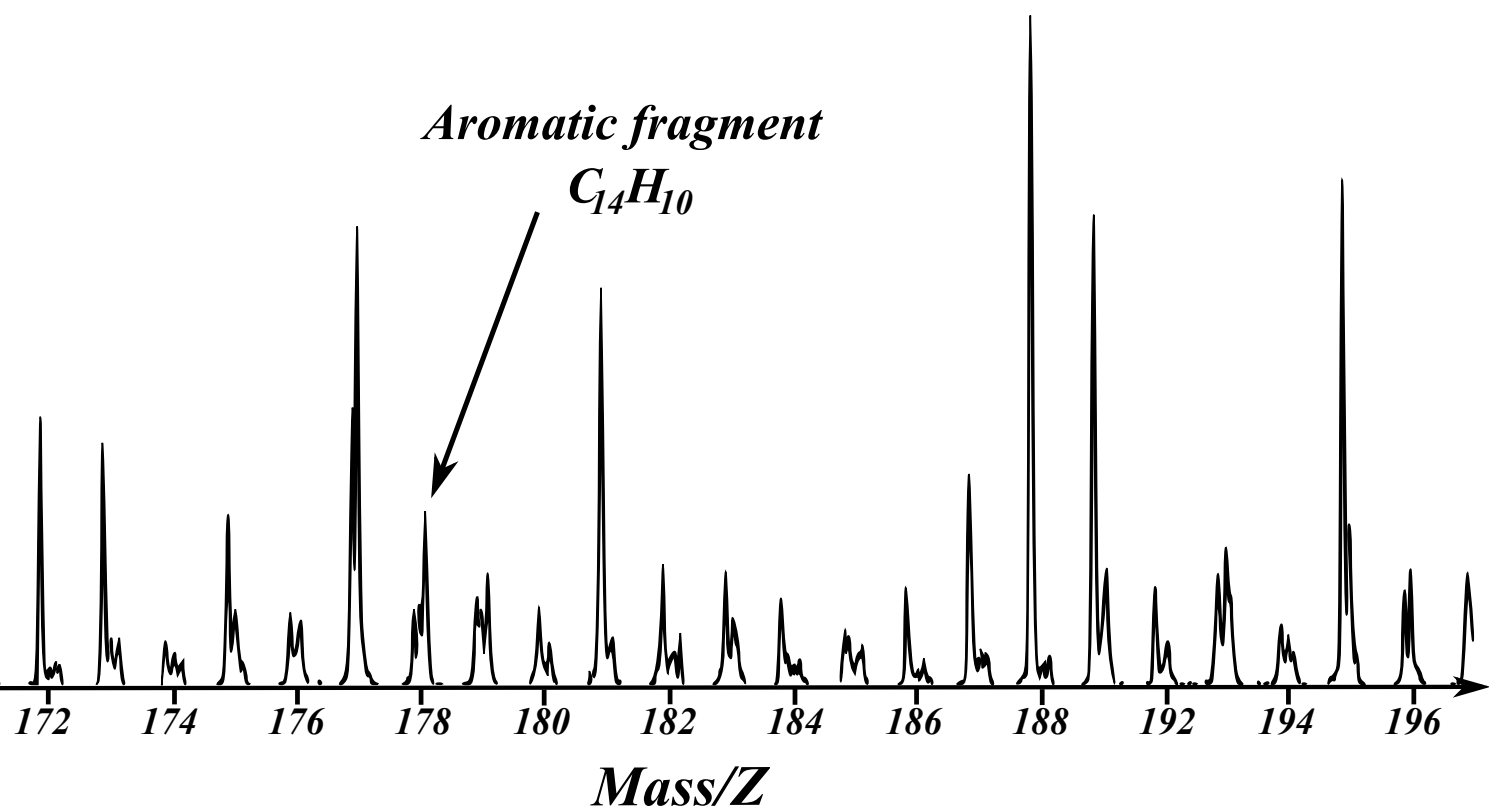
Aromatic fragment
$C_{14}H_{10}$
172
174
176
178
180
182
184
186
188
192
194
196
Mass/Z

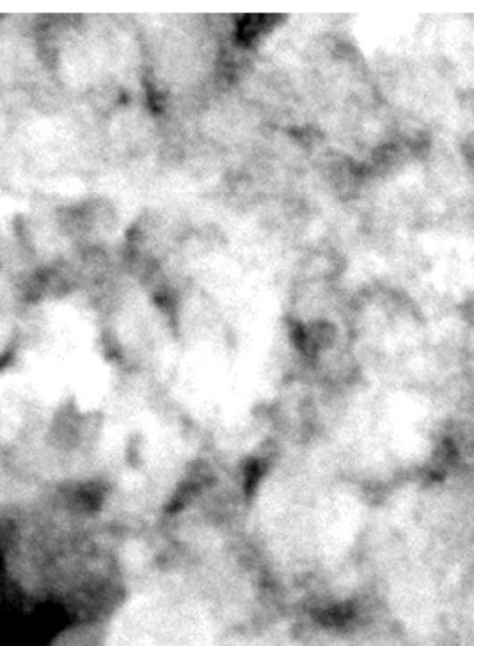

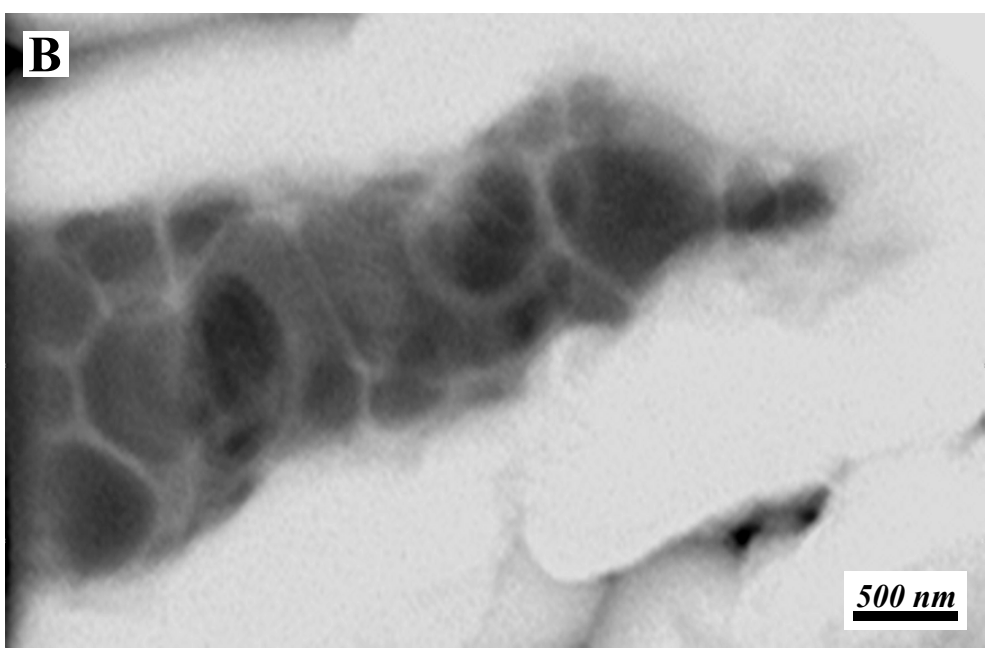
B
500 nm

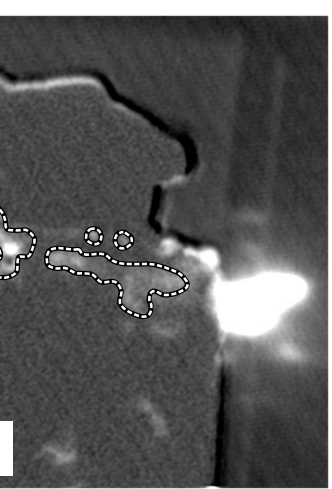

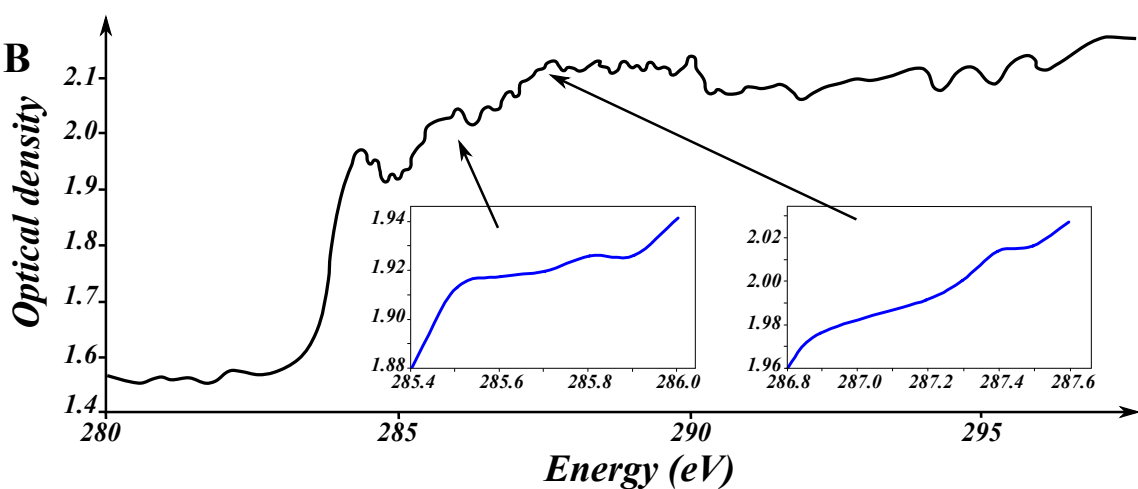
B
Optical density
2.1
2.0
1.9
1.8
1.7
1.6
1.4
280
285
290
295
Energy (eV)
1.94
1.92
1.90
1.88
285.4
285.6
285.8
286.0
2.02
2.00
1.98
1.96
286.8
287.0
287.2
287.4
287.6

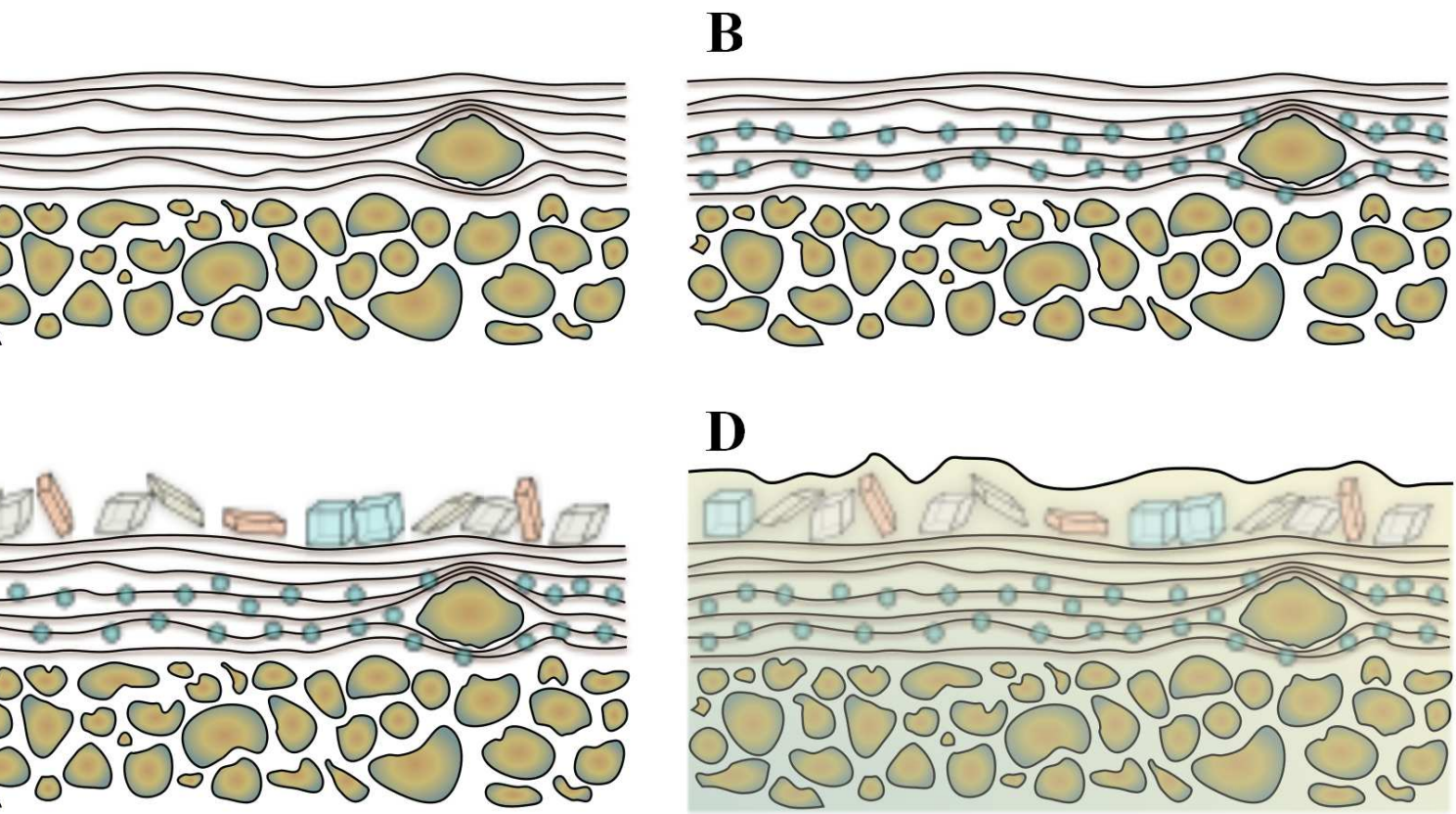

Caption

etrital particles

Microbial biofilm/mat

Nanocrystals of carbonate nucleated onto the EPS network in the degraded low portion of the mat

Evaporite minerals (halite, calcite, aragonite, gypsum) encrusting surface of biofilm

Silica coating and permeating the mat

GENERAL MAT CHARACTERISTICS		CHARACTERISTICS OF MODERN PHOTOSYNTHETIC MICROBIAL MATS	CHARACTERISTICS OF MODERN NON-PHOTOSYNTHETIC MICROBIAL MATS	MAJOR DIFFERENCES BETWEEN PHOTOSYNTHETIC (P) AND NON-PHOTOSYNTHETIC (NP) MICROBIAL MATS	CORRESPONDING CHARACTERISTICS IN THE JOSEFSDAL CHERT MICROBIAL FILM
ENVIRONMENT	**Water depth**	Photic zone	Non-photic/photic environment; shallow to deep water; can also form in association with photosynthetic mats	NP mats can form in non-photic zone	Formation in the photic zone;
	Environment type	Within photic zone, littoral marine, lacustrine	anaerobic chemosynthetic mats can form in cold seep, mud volcano, or hydrothermal vent area, also sulphide-rich caves		Littoral, tidal-supratidal environment
	Substrate	Formation on a surface (sediments/rocks/other)	Formation on a surface and within sediments	NP mats can form within sediments	Formation on a sediment surface
	Oxygen	Aerobic/anaerobic	Anaerobic but formation at oxic/anoxic interface obligatory for SOBs*		Anaerobic environment
	Temporal/spatial variability	Diurnal changes in vertical microbial composition (and metabolisms)	Temporal/spatial changes related to fluctuations in chemistry of fluid outflow		Not recorded
STRUCTURE	**Vertical stratigraphy**	Vertical stratigraphy in individual mats	Not described but vertical stratigraphy can be envisaged		Vertical stratigraphy; upper, active, non-calcified layer and lower, degraded calcified layer
	Lamination	Finely laminated structure of superimposed mats; wavy; domical; columnar	Finely laminated structure; wavy, vertical columns		Finely laminated structure; wavy
	Microbially-induced sedimentary structures (MISS)	MISS; sediment stabilisation; trapping; wrinkle structures; desiccation features	Sediment stabilisation, trapping; wrinkle features; downward growth into sediment following redox gradient	No exposure and desiccation described for NP mats	Formation under flowing water; overturning filaments, mat portions; desiccation; embedded evaporite mineral suite; sediment stabilisation
COMPOSITION	**Microbial**	Variable microbial composition related to redox gradient with depth in mat; phototrophic and heterotrophic; gliding microorganisms	S-oxidising bacteria (SOB); anaerobic CH_4 oxidisers; can also form in association with photosynthetic mats		EPS-secreting filaments (probably gliding), rods (cf. Westall et al., 2006)
	EPS	Large amounts of EPS	Can produce large amounts of EPS		Large amounts of EPS
	Distinctive lipid biomarkers	Specific molecular composition of photosynthesisers; e.g. chlorophyll (cyanobacteria), bacteriochlorophyl (anoxygenic photosynthesisers)	e.g. mono-O-alkyl glycerol ethers (many biomarkers overlap with those of photosynthesisers, e.g. hopanes)	Some biomarker differences	None preserved (organics are too old)
	Sulphur	S present (dissimilatory sulphate reduction)	Element S deposits from CH_4 oxidation	Elemental S only in NP mats	S-containing molecule thiophene, pyrite
	redox conditions	Roughly vertical distribution oxygenic above, anoxygenic below with dirunal variations	anaerobic for CH_4 oxidisers; redox gradient obligatory for SO_4 oxidisers		anaerobic (pyrite)
	Inorganic chemistry	Vertical distribution in solutes, nutrients, Eh, pH etc.	Vertical and spatial distribution in solutes, nutrients, Eh, pH etc.		Some vertical distribution indicated by the different characteristics of the top, non-calcified layer and the lower, calcified layer
METABOLIC SIGNATURES	**Carbon isotopes**	Variable depending upon dominating organism; mixed signature from bulk mat	Less variable (?); very light for methanogens	Bulk C isotopes of P mats are slightly heavier than thos of NP mats	δ13C ~-26.7‰
	***in situ* lithification**	Calcification (*N.B.* not all mats lithify), silicification in hot spring environments	Calcification (^{13}C-depleted in case of CH_4 oxidisers); phosphorites	Phosphoritisation in NP mats	*in situ* calcification
	Other metabolisms	Other metabolisms, sulphate reduction/oxidation, methanogenesis	sulphate-reduction, methanogenesis		Possible sulphur reduction

* SOB: sulphate oxidising bacteria